Aalto-yliopisto
Insinööritieteiden
korkeakoulu

Olli Niiranen

Evaluation of a Two-Scale Model for Composite and Plywood Plates

Master's thesis submitted in partial fulfillment of the requirements for the degree of Master of Science in Technology

Espoo, August 19th, 2016
Thesis supervisor: Professor Jukka Tuhkuri
Thesis advisor: D.Sc. Jouni Freund

Aalto-yliopisto
Insinööritieteiden
korkeakoulu

Aalto-yliopisto, PL 11000, 00076 AALTO
www.aalto.fi

Diplomityön tiivistelmä

Tekijä Olli Niiranen		
Työn nimi Kaksiskaalamallin soveltuvuus komposiitti- ja vanerilaatoille		
Koulutusohjelma Konetekniikka		
Pää-/sivuaine Lentotekniikka/Koneensuunnittelu		**Koodi** K3004/K3001
Työn valvoja Professori Jukka Tuhkuri		
Työn ohjaaja(t) TkT Jouni Freund		
Päivämäärä 19.08.2016	**Sivumäärä** 76	**Kieli** Englanti

Tiivistelmä

Tässä työssä on tutkittu uuden kaksiskaalaisen laattamallin tarkkuutta verrattuna tarkkaan kolmiulotteiseen elastisuusratkaisuun sekä muokkaamattomaan Reissner-Mindlin -laattamalliin erikokoisilla, -rakenteisilla ja -muotoisilla laatoilla. Tutkimuksen tavoitteena oli mallin tarkkuuden tarkastelemisen lisäksi selvittää uuden mallin soveltuvuus vaneristen levyjen jännitysten ja siirtymien analysoimiseen. Uudelta mallilta vaadittiin selkeästi parempi tarkkuus kuin Reissner-Mindlin -mallilta, jotta mallin käyttö olisi perusteltua.

Työssä esitellään aluksi vaneri materiaalina, ortotrooppisen komposiittilevyn laskemiseen liittyvät erityispiirteet sekä esitellään Reissner-Mindlin -malli ja työssä tutkittu kaksiskaalainen laattamalli. Tämän jälkeen käsitellään työssä tehdyissä vertailuissa käytetty kuormitus, reunaehdot, vertailtavien mallien käyttö vertailutulosten ratkaisemiseksi sekä vertailusta saadut tulokset. Työn lopuksi käsitellään tulosten pohjalta tehtyjä johtopäätöksiä ja mahdollisuuksia jatkotutkimukseen.

Tehdyn vertailun perusteella uusi kaksiskaalainen laattamalli on selkeästi Reissner-Mindlin -mallia tarkempi. Tämän lisäksi uusi malli kykenee mallintamaan levynsisäisten jatkuvien leikkausjännitysten jakaumat huomattavasti Reissner-Mindlin -mallia tarkemmin. Malli todettiin erityisen tarkaksi vanerilevyjen yleisimpien mittojen alueella.

Avainsanat Laatta, malli, laattamalli vaneri, komposiitti, Reissner-Mindlin, kaksiskaalainen, ortotropia, anisotropia, laattateoria, lujuusoppi, elastisuus, elastisuusratkaisu, jännitys, siirtymä

Aalto University
School of Engineering

Aalto University, P.O. BOX 11000, 00076 AALTO
www.aalto.fi

Abstract of master's thesis

Author Olli Niiranen		
Title of thesis Evaluation of a two-scale model for composite and plywood plates		
Degree programme Mechanical Engineering		
Major/minor Aeronautical Engineering/Machine Design		**Code** K3004/K3001
Thesis supervisor Professor Jukka Tuhkuri		
Thesis advisor(s) D.Sc. Jouni Freund		
Date August 19th, 2016	**Number of pages** 76	**Language** English

Abstract

This thesis evaluates the accuracy of a new two-scale plate model against a three dimensional elasticity solution and the unmodified Reissner-Mindlin plate model for plates with different sizes, layups and forms. The aim of this research was also to evaluate the suitability of the model for the analysis of plywood plates. The two-scale model was required to have improved accuracy over the unmodified Reissner-Mindlin model, to warrant its use.

The thesis will begin with a discussion of plywood as a material and how orthotropic materials, such as plywood plates, are analyzed. The new two-scale plate model and the Reissner-Mindlin model are also described briefly. The evaluation part of the thesis begins with descriptions of the loading and boundary conditions of the plate, as well as a description on how the models were used in the evaluations, and continues with the results. At the end of this thesis, conclusions based on the evaluations and possibilities for future research are presented.

Based on the evaluations, the new two-scale model is more accurate than the Reissner-Mindlin model, and capable of modeling the continuous stress distributions far more accurately. The new model was found to be especially accurate in the dimensions typically found in plywood.

Keywords Plate, model, plate model, plywood, composites, Reissner-Mindlin, two-scale, orthotropy, anisotropy, plate theory, solid mechanics, elasticity, elasticity solution, stress, displacement

Foreword

This thesis was written for the Aalto University Department of Applied Mechanics during spring 2016. The aim of this study was to evaluate a new two-scale plate model against an exact three dimensional elasticity solution and the Reissner-Mindlin plate model as well as determining the suitability of the new model for analysis of plywood plates. The supervisor of this thesis was Professor Jukka Tuhkuri and the advisor of this thesis was Doctor Jouni Freund, both from the Aalto University Department of Applied Mechanics.

I wish to thank Professor Jukka Tuhkuri for being my supervisor and Doctor Jouni Freund for the excellent guidance and kind and valuable feedback he provided. I would also like to thank R&D Manager Anu Huovinen from Metsä Wood for all the valuable information on plywood.

Finally, I thank my family and friends for their support and interest towards my thesis.

Espoo, August 19th, 2016

Olli Niiranen

Table of Contents

List of Symbols

E	[Pa]	Modulus of elasticity, also known as Young's modulus
G	[Pa]	Shear modulus
H	[m]	Width of a plate
L	[m]	Length of a plate
M	[Nm/m]	Internal moment acting in a plate
N	[N/m]	Internal normal force acting in a plate
Q	[N/m]	Internal shear force acting in a plate
S	[Pa]	Elasticity parameter in xy-system
U, V, W		Displacement in the small direction in a plate
U	[J]	Potential energy of a plate
U_{int}	[J]	Internal potential energy of a plate
W_{ext}	[J]	Work of external forces
a_1, a_2, a_3		Unknowns in the standard solution
b	[N/m]	External surface force acting on a plate
c	[N/m]	External shear force acting on a plate
$\vec{e}_i$		Unit vector in the direction of a plies principal axis
$\vec{f}$		Variable used in the solution of the refined model
$\vec{i}$		Unit vector in the x-axial direction
$\vec{j}$		Unit vector in the y-axial direction
$\vec{k}$		Unit vector in the z-axial direction
n		Number of plies in a laminate
$\vec{q}, q$	[N/m]	External surface force
q_0	[N/m]	External force magnitude
t	[m]	Thickness of a plate
t_i, h	[m]	Thickness of a ply

$\vec{t}$	[N/m]	External surface force
u		Displacement in the direction of the x-axis
v		Displacement in the direction of the y-axis
w		Displacement in the direction of the z-axis
z	[m]	Location of a particle or a plane on the z-axis
α	[°]	The lay-up angle of a ply
β		Ratio of a material's elastic moduli
χ		Ratio of a material's Poisson's ratio
δ		Ratio of a material's shear moduli
Δu		x component of warping displacement
Δv		y component of warping displacement
Δw		z component of warping displacement
ε		Strain
ϕ		Rotation around the x-axis
γ		Aspect ratio of a plate
η		Thickness ratio of a plate
$\vec{\lambda}_0$		Lagrange multiplier
μ		Loading ratio of a plate
ν		Poisson's ratio
θ		Rotation around the y-axis
σ	[Pa]	Stress
$\vec{\sigma}$		Stress vector
$\vec{\vec{\sigma}}$		Second-order stress dyad
$\boldsymbol{\sigma}$		xyz-coordinate system components of the stress dyad

1 Introduction and notations

1.1 Introduction

A plate is a solid object with two principal dimensions that are greater than the third. The importance of plate-like components in structural applications is significant due to the fact that they can be used to make structures that are light, yet rigid; they provide aerodynamic skins for wings and sturdy surfaces for vehicles to move on. In fact, plates can be found nearly everywhere, from the plywood plate covered access ramps at a construction site to the carbon-fiber reinforced skin panels on aircraft's wings, from the steel plate bulkheads in a ship to the complex sandwich plate hull of a satellite. Plates can even be found at homes and workplaces in the form of table tops and shelves. With such a wide range of applications, it is easily seen that the ability to reliably estimate the stresses acting inside a plate is required to ensure that the structure is safe in normal use. Alternatively, it would be possible to simply overengineer the structure to ensure the durability of the plate, but this would also cause the plate to become unnecessarily heavy. In many applications, the weight and size of a component are severely limited due to the operating costs of the device, which may lead to operating conditions that are close to the failure stresses of the material. Accurate calculations become especially critical in these kinds of applications, as they usually also incorporate requirements on the reliability and safety of the device. Applications with such requirements often need careful optimization of the structure, which means that the accuracy of the stresses acting in each direction becomes all the more important. Figures 1 to 3 illustrate some applications of plates.

Figure 1. The layered structure of a plywood plate used as the surface of a flatbed trailer, a metallic and a plywood plate used as traffic signs.

Figure 2. A plywood plate used as a temporary wall at a construction site and the glass façade of a building.

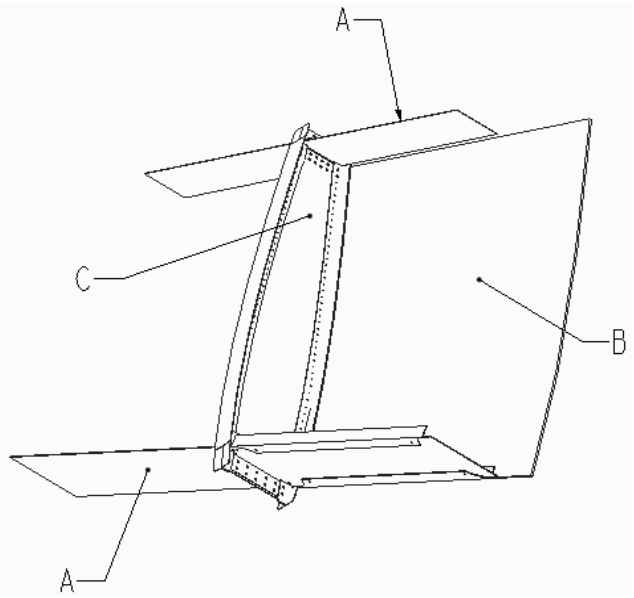

Figure 3. The Structure of a wing, illustrated from below, contains many plate components such as the wing spars (A), the skin plates (B) and the web plates of the wing ribs (C).

In composite materials, the mechanical properties can be tailored to suit the application by adjusting the lay-ups and fiber directions. With non-homogenous materials, the arising problem is that unlike isotropic and homogenous materials like metals, there exists more failure modes than the yielding and breaking of homogenous materials. Composite materials such as plywood and carbon-fiber reinforced plastic can yield and break like metals in axial loading, but they can also fail through shearing of the bonding material between the plies and through peeling of the layers. Because of this, traditional models such as the Reissner-Mindlin plate model, which assumes that the plate has no internal stresses acting in the direction of the thickness of the plate, cannot be used to safely solve the durability of a plate loaded in the z-axial direction. Another weakness of the traditional models is that they assume that the shear stresses are constant over the thickness of the plies, which is not true. Using the previous assumption will lead to solutions giving either too high or too low local stresses compared to the actual values found in plates. As plates are used in many applications where the accuracy of calculations is important, a need for increasingly accurate methods to calculate the stresses and strains in these components has arisen. [Kant & Swaminathan, 2002]

The first plate model was developed by Kirchhoff during the 19th century. This classical laminated plate theory was based on the displacement field and assumed that lines normal to the mid-plane at equilibrium remain straight lines and normal to the plane during deformation. While this model is simple to solve and calculate, it ignores the effects of transverse strain on the deformation of a plate. In fact this is one of the greatest problems of the classical laminated plate theory, as especially composite plates are subjected to transverse shear stresses that may significantly contribute to the plate's failure and deflection. However, due to the relative simplicity and ease of calculation, this model is still quite commonly used for quick estimates for plate behavior. [Khandan et al., 2012][Carrera, 2000][Kant & Swaminathan, 2002]

An improvement over the classical plate theory is achieved with first-order shear deformation theories. The basic theory was developed by Reissner and Mindlin, which is why the most common model is known as the Reissner-Mindlin model. This model has an advantage over the classical plate theory in that it allows the normal line-segments to move more freely in deformation and thereby the assumptions of the model are not as severe as

those of the Kirchhoff plate theory. However, the Reissner-Mindlin model still has a weakness in that it assumes that the displacements in the direction of the plate's thickness and the transverse shear stresses are constant. Another weakness of the model is that it is also incapable of solving the stresses in the direction of the thickness of the plate, as the normal stress component in this direction is assumed to be zero. With the above assumptions, the model provides results that would indicate that the plate is more rigid than it actually is, causing inaccuracies in both the displacements and stresses of the plate. A shear correction factor can be used to adjust the stiffness to better match the actual properties but the accuracy of the stresses may still be poor [Ferreira et al., 2003][Kapuria and Kulkarni, 2007][Kant & Swaminathan, 2002]. [Khandan et al., 2012][Cho & Averill, 1997][Matsunaga, 2002]

Layerwise theories provide a way to solve the zig-zag behavior of the in-plane displacements in the direction of the thickness of the plate [Brischetto et al., 2009]. These theories are also known as zig-zag theories due to the form of their solutions. Behind these models is the assumption of certain displacement and stress distributions in the layers of the plate that are tied together at the interfaces by equilibrium and compatibility equations. The advantage of these models is that they can satisfy both the shear stress continuity conditions and the requirement of stress-free upper and lower surfaces. However, this class of models tends to become rather heavy at higher numbers of plies, as the number of equations is directly proportional to the number of plies. [Khandan et al., 2012][Carrera, 2004][Cho & Averill, 1997][Mantari et al., 2012].

Limitations of the previous models have led to the development of a number of higher-order shear deformation theories [Kant & Swaminathan, 2002]. While the zig-zag theories solve the stresses and strains separately at each layer, the higher-order shear deformation theories make use of unknowns depending on the mid-surface coordinates only in the same manner as the classical theories. The basis of these higher-order theories is an assumption of nonlinear stress variation through the thickness of the plate. Using this assumption instead of those of the two previous models provides a major improvement in accuracy because the model can now display the warping of the line segments in deformation. However, a major weakness of the higher-order shear deformation theories is that the more accurate models are rather labor-intensive, while some of the less complex ones do not

provide results satisfying the continuity conditions of the layer interfaces [Matsunaga, 2002]. [Khandan et al., 2012][Carrera, 2001]

A two-scale plate model suggested in [Freund, 2016] aims to combine simplicity and accuracy in a more favorable manner than the zig-zag and higher order theories in literature. The aim of this thesis is the evaluation of the two-scale model for composite and plywood plates against the Reissner-Mindlin model and an exact solution by Pagano with varying geometric and material parameters. In more precise terms, this means that the goal is to find the range of size, shape and materials, where the two-scale model provides a significant improvement in accuracy over the standard model. Compared models are presented in the following list:

1. The standard model, used as the baseline for the accuracy of non-exact solutions, is the standard Reissner-Mindlin model. It is a first-order shear deformation theory and provides quick results.

2. The new two-scale model [Freund, 2016] combines the standard Reissner-Mindlin model with a higher-order shear deformation model. This refined model provides improved accuracy for the solving of the displacements and stresses in a plate with only a modest increase in complexity.

3. The absolute accuracy of the two plate theories that are discussed in this thesis will be compared to an exact solution by N. J. Pagano [1969]. Pagano's solution is based on an elasticity solution for plates and it provides accurate results within the linear elasticity theory.

This thesis investigates the effects that increasing the number of layers of a plate as well as altering the aspect ratio and relative thickness of the plate have on the accuracy of the new model. The effect of the material parameters on the accuracy is also evaluated. However, the scope is limited to the investigation of geometric and material parameter values that are typical for plywood as well as the material parameters of an extremely orthotropic material and an isotropic material. Limitations are also placed on the boundary conditions, as the effects of the plate's attachments and the proximity of edges on the accuracy of the refined

model is not evaluated. The external load used in the evaluations is also fixed, as it is kept as a sinusoidal distributed traction that acts on the entire upper surface of the plate. This is done partially because of the available exact solution by Pagano [1969], which specifies the external loading and the supports at the edges.

A presentation of the standard Reissner-Mindlin plate model and plywood as a material is given in chapters 3 and 2 respectively. Included in the presentation are the important steps of the derivation of the standard model from the kinematic and kinetic assumptions of the model. After the standard model is presented, a two-scale model for plates is discussed [Freund, 2016].

Evaluation of the standard and two-scale models is performed with an analytical version of Pagano's model. This exact solution is one that is commonly used in literature as a baseline for the evaluation of the accuracy of new models [Mantari et al., 2012][Kapuria and Kulkarni, 2007][Kant & Swaminathan, 2002][Matsunaga, 2002]. The results of the evaluation are given as graphs, where the results of the three models are plotted together to provide a visual representation of the accuracies of the models, as well as tables, with the modeling error of the Reissner-Mindlin and the two-scale theories given as the L_2 norm of the models against the exact solution. At the end of the thesis, the results of the evaluation are discussed and the new model's suitability for different cases is discussed.

Although the focus of this text is on plywood, the models presented in this thesis can also be used for any other material, such as fiber reinforced composites and metallic materials.

1.2 Notations

Multiple types of notations have been developed for use in science and technology of which the component notation and dyadic notation will be used in this thesis. The majority of equations that are used are in component notation, as this form is more accessible and clearer. On the other hand, deriving certain equations require tools that are better suited for long and complicated equations. Therefore the appendices use tensor and dyadic notation for the deriving of the elasticity matrix in the xy-coordinate system.

Symbols written in *italic* are scalars, such as length, stress components and the modulus of elasticity to name a few. Vectors and dyads are written in italic, but they also have an arrow with single or double heads on top of the symbol. Matrices, representing the components of vectors and dyads, are denoted by symbols written in **bold**.

Examples of the different symbol types are given as follows; the stress component acting in the x-axial direction of the plane normal to the x-axis is written as σ_{xx}, the stress vector acting in the plane normal to the x-axis is $\vec{\sigma}_x$, the notation for the second-order stress dyad in the xyz-coordinate system is $\vec{\vec{\sigma}}$ and the xyz-coordinate system components of the dyad are written as $\boldsymbol{\sigma}$.

To provide a better view of the relations between the different notations and symbols, the following example involving the stress dyad is provided. First, the second-order stress dyad and its components are related by

$$\vec{\vec{\sigma}} = \begin{Bmatrix} \vec{i} \\ \vec{j} \\ \vec{k} \end{Bmatrix}^T \boldsymbol{\sigma} \begin{Bmatrix} \vec{i} \\ \vec{j} \\ \vec{k} \end{Bmatrix} = \begin{Bmatrix} \vec{i} \\ \vec{j} \\ \vec{k} \end{Bmatrix}^T \begin{bmatrix} \sigma_{xx} & \sigma_{xy} & \sigma_{xz} \\ \sigma_{yx} & \sigma_{yy} & \sigma_{yz} \\ \sigma_{zx} & \sigma_{zy} & \sigma_{zz} \end{bmatrix} \begin{Bmatrix} \vec{i} \\ \vec{j} \\ \vec{k} \end{Bmatrix} \tag{1}$$

in which $\vec{i}$, $\vec{j}$ and $\vec{k}$ are the unit vectors in the directions of the xyz-coordinate system's axes and σ is the symbol for a stress component.

The dyad notation is a form of mathematical notation, where equations are written in terms of the unit vectors of the xyz-coordinate system. The alternative form of the stress dyad [Chou & Pagano 1967, page 237]

$$\vec{\vec{\sigma}} = \vec{i}\vec{i}\,\sigma_{xx} + \vec{i}\vec{j}\,\sigma_{xy} + \vec{i}\vec{k}\,\sigma_{xz} + \vec{j}\vec{i}\,\sigma_{yx} + \vec{j}\vec{j}\,\sigma_{yy} + \vec{j}\vec{k}\,\sigma_{yz} + \vec{k}\vec{i}\,\sigma_{zx} + \vec{k}\vec{j}\,\sigma_{zy} + \vec{k}\vec{k}\,\sigma_{zz} \ , \tag{2}$$

can be obtained by expanding the last form in equation (1).

Continuing with the example, the stress vector can be defined using the stress dyad as follows

$$\vec{\sigma} = \vec{k} \cdot \vec{\vec{\sigma}} = \begin{Bmatrix} \sigma_{zx} \\ \sigma_{zy} \\ \sigma_{zz} \end{Bmatrix}^T \begin{Bmatrix} \vec{i} \\ \vec{j} \\ \vec{k} \end{Bmatrix} . \tag{3}$$

Dyad notation uses mostly the same rules for calculation as normal vector algebra, but there exists one major difference between the two. Unlike when working with traditional vectors, it is now possible to multiply two vectors to produce forms as the one shown in equation (2), which would not be allowed in normal vector calculus. In dyad notation it is also extremely important to maintain the exact order of the unit vectors, as they are not interchangeable. For example [Chou & Pagano 1967, page 231]

$$\vec{i}\vec{j} \neq \vec{j}\vec{i} . \tag{4}$$

Although the dyad notation is more suitable for deriving equations in solid mechanics, traditional component notation is the primary notation used in this thesis. This decision is made to provide clearer and more easily usable equations, which will also provide easier access to the results of this thesis. Still, the increased simplicity of the dyad notation when dealing with more complicated equations is enough to justify the use of this notation in the appendices, where the derived equations become quite long.

2 Plywood material

2.1 Plywood plate material model

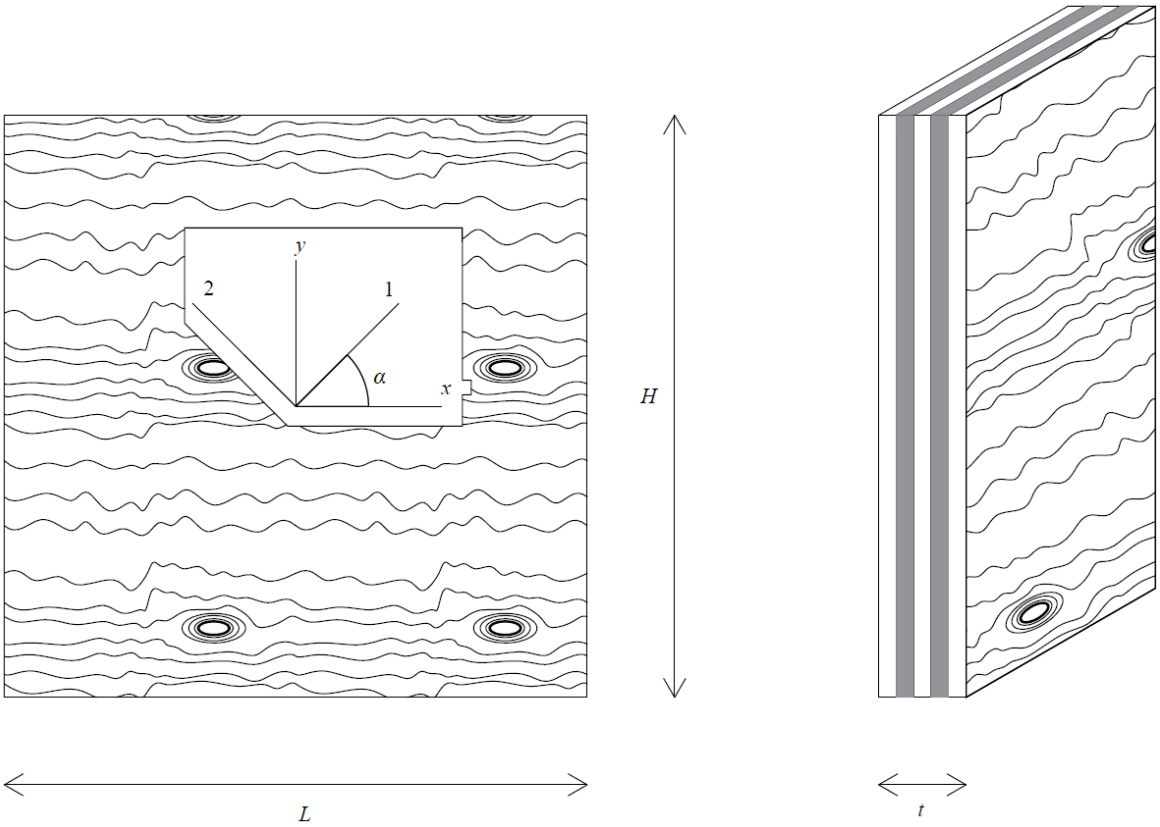

Figure 4. The structure of a plywood plate.

Plywood is a composite material, which consists of multiple wooden plies stacked on each other, as shown in Figure 4, to form a plate with the desired properties. Due to the direction dependent nature of the material properties of wood, plywood has different parameters in different directions. Materials that have properties like this are called orthotropic, that is, their properties differ in the three orthogonal directions. To represent the combined properties of a plywood plate, it is convenient to use two coordinate systems. The first, ply coordinate system $(1,\ 2,\ 3)$, is that of a single ply, oriented so that one axis (1) is parallel to the fibers, one axis perpendicular to the fibers (2) and one axis so that it is normal to the plane formed by the ply's surface (3). On the other hand, the plate coordinate system $(x,\ y,\ z)$ should be defined as a global coordinate system that remains constant, independent of the orientation of the plies. Due to the constant nature of the global

coordinate system, it is possible to convert the local material properties from plies to direction dependent global properties. This conversion significantly reduces the work required in the representation of the plywood plate material properties.

All equations presented in this thesis assume that the elasticity theory is valid, that is, the effects of permanent deformation and strain hardening are considered to be non-existent. This allows Hooke's law to be used in the relation between stresses and strains. These assumptions are acceptable when comparing different models, with each model having the same assumptions, but should not be used in real applications where the effects of plastic deformation may no longer be omitted. In practice, the assumption is acceptable when the permanent strains in an object are less than 0,2 % or the stresses are below the yield limit, whichever is applicable to the material in question [Ashby & Jones, 2012, page 36].

In an orthotropic material, the stress-strain relationship can be modified from the form shown by Lee & Suh [2006, page 83] to provide the following forms

$$\begin{Bmatrix} \sigma_{11} \\ \sigma_{22} \\ \sigma_{33} \end{Bmatrix} = \begin{bmatrix} \frac{1}{E_1} & \frac{-\nu_{21}}{E_2} & \frac{-\nu_{31}}{E_3} \\ \frac{-\nu_{12}}{E_1} & \frac{1}{E_2} & \frac{-\nu_{32}}{E_3} \\ \frac{-\nu_{13}}{E_1} & \frac{-\nu_{23}}{E_2} & \frac{1}{E_3} \end{bmatrix}^{-1} \begin{Bmatrix} \varepsilon_{11} \\ \varepsilon_{22} \\ \varepsilon_{33} \end{Bmatrix} \tag{5}$$

and

$$\begin{Bmatrix} \sigma_{12} \\ \sigma_{23} \\ \sigma_{31} \end{Bmatrix} = \begin{bmatrix} \frac{1}{G_{12}} & 0 & 0 \\ 0 & \frac{1}{G_{23}} & 0 \\ 0 & 0 & \frac{1}{G_{13}} \end{bmatrix}^{-1} 2 \begin{Bmatrix} \varepsilon_{12} \\ \varepsilon_{23} \\ \varepsilon_{31} \end{Bmatrix}. \tag{6}$$

In the equations the symbols σ and ε signify the stresses and strains respectively and the subscripts signify the components of the stress or strain. Stress is defined as the effect that a force acting on a plane has on an object. In its simplest form, stress is caused by an axial

force acting on a rod and is defined as the force divided by the cross-sectional area of the rod. Strain quantifies the material element shape distortion. In the simplest case of a rod, deformation can be defined as the length change divided by the original length of the rod. Young's modulus, symbolized by E, is a measure of rigidity and the subscript signifies the direction for the property of the material. Young's modulus, which is also known as the modulus of elasticity, signifies the relation that exists between stress and strain. The modulus could be thought of as the spring constant of materials, as it relates the amount an object deforms for a given load. Respectively, the symbol G signifies the shear modulus and the subscripts signify the direction of the modulus. In practice, the shear modulus is similar to the Young's modulus but instead of acting in one of the principal directions, such as the x-, y- or z-axis, it links the shear forces into shear strain, causing for instance a rectangular object to deform into a parallelogram under shear forces. Poisson's ratio ν is a material dependent constant that links deformations from one plane to another. This constant is used to take into account, for instance, the reduction in cross-sectional area of a rod deformed in axial tension.

The form required by the engineering models can be derived starting from equations (5) and (6). In the standard plate model, the constitutive equation should satisfy the kinetic assumption; this assumption will be discussed further in Chapter 3.2, but can already be used in the derivation presented here. Substituting the condition that $\sigma_{33} = 0$ into equation (5) allows the equation to be written as

$$\begin{Bmatrix} \sigma_{11} \\ \sigma_{22} \\ \sigma_{33} \end{Bmatrix} = \frac{1}{1-\nu_{21}\nu_{12}} \begin{bmatrix} E_1 & \nu_{21}E_1 & 0 \\ \nu_{12}E_2 & E_2 & 0 \\ 0 & 0 & 0 \end{bmatrix} \begin{Bmatrix} \varepsilon_{11} \\ \varepsilon_{22} \\ \varepsilon_{33} \end{Bmatrix}. \tag{7}$$

Constitutive equations (6) and (7) expressed in the xyz-coordinate system provide the following equations

$$\begin{Bmatrix}\sigma_{xx}\\ \sigma_{yy}\\ \sigma_{xy}\end{Bmatrix}=\begin{bmatrix}S_1 & S_3 & S_7\\ S_3 & S_2 & S_8\\ S_7 & S_8 & S_4\end{bmatrix}\begin{Bmatrix}\dfrac{\partial u_x}{\partial x}\\ \dfrac{\partial u_y}{\partial y}\\ \dfrac{\partial u_x}{\partial y}+\dfrac{\partial u_y}{\partial x}\end{Bmatrix} \tag{8}$$

and

$$\begin{Bmatrix}\sigma_{yz}\\ \sigma_{zx}\end{Bmatrix}=\begin{bmatrix}S_5 & S_9\\ S_9 & S_6\end{bmatrix}\begin{Bmatrix}\dfrac{\partial u_z}{\partial y}+\dfrac{\partial u_y}{\partial z}\\ \dfrac{\partial u_x}{\partial z}+\dfrac{\partial u_z}{\partial x}\end{Bmatrix}. \tag{9}$$

In equations (8) and (9), the strains used in equations (6) and (7) are written in terms of the derivatives of the displacement components and the symmetry of the off-diagonal terms ($\sigma_{xy}=\sigma_{yx}$, $\sigma_{zx}=\sigma_{xz}$ and $\sigma_{yz}=\sigma_{zy}$) has been taken into account. In later calculations, displacement components will be replaced by their plate representations consisting of translation and rotation parts.

Using matrix representation, the S terms of the elasticity parameters of the plate coordinate system in equations (8) and (9) are

$$\begin{Bmatrix}S_1\\ S_2\\ S_3\\ S_4\\ S_7\\ S_8\end{Bmatrix}=\begin{bmatrix}\mathrm{c}^4 & \mathrm{s}^4 & 2\mathrm{s}^2\mathrm{c}^2 & 4\mathrm{c}^2\mathrm{s}^2\\ \mathrm{s}^4 & \mathrm{c}^4 & 2\mathrm{s}^2\mathrm{c}^2 & 4\mathrm{c}^2\mathrm{s}^2\\ \mathrm{c}^2\mathrm{s}^2 & \mathrm{c}^2\mathrm{s}^2 & \mathrm{c}^4+\mathrm{s}^4 & -4\mathrm{c}^2\mathrm{s}^2\\ \mathrm{c}^2\mathrm{s}^2 & \mathrm{c}^2\mathrm{s}^2 & -2\mathrm{c}^2\mathrm{s}^2 & \mathrm{s}^4-2\mathrm{c}^2\mathrm{s}^2+\mathrm{c}^4\\ \mathrm{c}^3\mathrm{s} & -\mathrm{c}\mathrm{s}^3 & -\mathrm{c}^3\mathrm{s}+\mathrm{c}\mathrm{s}^3 & 2\mathrm{c}\mathrm{s}^3-2\mathrm{c}^3\mathrm{s}\\ \mathrm{c}\mathrm{s}^3 & -\mathrm{c}^3\mathrm{s} & -\mathrm{c}\mathrm{s}^3+\mathrm{c}^3\mathrm{s} & 2\mathrm{c}^3\mathrm{s}-2\mathrm{c}\mathrm{s}^3\end{bmatrix}\begin{Bmatrix}\dfrac{E_1}{1-\nu_{21}\nu_{12}}\\ \dfrac{E_2}{1-\nu_{21}\nu_{12}}\\ \dfrac{\nu_{21}E_1}{1-\nu_{21}\nu_{12}}\\ G_{12}\end{Bmatrix} \tag{10}$$

and

$$\begin{Bmatrix}S_5\\ S_6\\ S_9\end{Bmatrix}=\begin{bmatrix}\mathrm{c}^2 & \mathrm{s}^2\\ \mathrm{s}^2 & \mathrm{c}^2\\ -\mathrm{c}\mathrm{s} & \mathrm{s}\mathrm{c}\end{bmatrix}\begin{Bmatrix}G_{23}\\ G_{31}\end{Bmatrix}, \tag{11}$$

in which $c = \cos(\alpha)$ and $s = \sin(\alpha)$, with α being defined in Figure 4. The important parts of the derivation of equations (10) and (11) are given in appendices A.1. and A.2.

2.2 Material parameters

Wood has the same material parameters as all materials, that is, the Young's modulus also known as the modulus of elasticity, the shear modulus and the Poisson's ratio. The difference between wood and metallic materials is that wood has different values for the properties in different material directions. For instance, wood is far more rigid in the direction parallel to the fibers than in the direction perpendicular to the fibers.

Literature, such as Mahoney [2000] and Forest Products Laboratory [2001], gives the material parameters of wood as functions of the longitudinal elastic modulus or the modulus in the direction of the fibers given by, for example, bending tests of wood specimens. Tables 1 and 2 show the ratios given by Mahoney [2000, pages (4-6) - (4-24)] and Forest Products Laboratory [2001, page 4-2] for certain wood types. The Poisson's ratios for the different wood types are given in Table 3. The values of the ratios provided by Mahoney [2000, pages (4-6) - (4-24)] and Forest Products Laboratory [2001, page 4-3] are in agreement.

Table 1. Material parameter ratios according to [Mahoney, 2000, pages (4-6) - (4-24)].

Material	E_2 / E_1	E_3 / E_1	G_{12} / E_1	G_{32} / E_1	G_{13} / E_1
Birch (Yellow)	0,050	0,078	0,068	0,017	0,074
Spruce (Sitka)	0,043	0,078	0,061	0,003	0,064
Douglas fir	0,050	0,068	0,078	0,007	0,064

Table 2. Material parameter ratios according to Forest Products Laboratory [2001, page 4-2].

Material	E_2 / E_1	E_3 / E_1	G_{12} / E_1	G_{32} / E_1	G_{13} / E_1
Birch (Yellow)	0,050	0,078	0,068	0,017	0,074
Spruce (Sitka)	0,043	0,078	0,061	0,003	0,064
Douglas fir	0,050	0,068	0,078	0,007	0,064

Typical values for the material parameters of different types of wood are given in Table 3. The values have been calculated from the previously given ratios and the average of the values for dry wood given by Mahoney [2000, pages (4-6) - (4-24)]. The values for steel, which is an isotropic material, were taken from Callister & Rethwisch [2011] and the shear modulus was solved using the following equation for isotropic materials [Callister & Rethwisch, 2011, page 161]

$$G_{Steel} = \frac{E_{Steel}}{2\left(1+\nu_{Steel}\right)} \ . \tag{12}$$

Table 3. Material parameters according to Mahoney [2000, pages (4-6) - (4-24)] and Callister & Rethwisch [2011, pages A6 - A10].

Material	E_1 [GPa]	E_2 [GPa]	E_3 [GPa]	G_{12} [MPa]	G_{23} [MPa]	G_{31} [MPa]	ν_{12}	ν_{13}	ν_{32}
Birch (Yellow)	13,86	0,693	1,081	942,4	235,6	1026	0,45	0,43	0,70
Spruce (Sitka)	10,82	0,465	0,844	660,3	32,47	692,8	0,47	0,37	0,44
Douglas fir	12,17	0,608	0,828	949,2	85,18	778,8	0,45	0,29	0,39
Steel AISI 4140	207	207	207	79620	79620	79620	0.3	0.3	0.3

The symmetry conditions

$$\frac{E_1}{\nu_{12}} = \frac{E_2}{\nu_{21}},$$

$$\frac{E_1}{\nu_{13}} = \frac{E_3}{\nu_{31}} \tag{13}$$

and

$$\frac{E_2}{\nu_{23}} = \frac{E_3}{\nu_{32}}$$

required by classical linear elasticity theory, provide the three missing Poisson's ratios.

Due to the existence of symmetry, only the principal Poisson's ratios ν_{12}, ν_{13} and ν_{32} are given in Table 3.

The values for the parameters presented in Table 3 clearly demonstrate the orthotropic nature of wood, as the modulus of elasticity is significantly greater in the direction parallel to the grains than in the directions normal to the grains. This would allow adjusting the mechanical properties of a plywood plate through orienting plies to be parallel with the load, as this would provide the least amount of axial deformation. On the other hand, by suitably orienting different plies, it would be possible to achieve a wide range of values for the stiffness and durability of a plate.

A simplified six parameter model will be used later in the examples section instead of the full 9 parameter model. Material parameters $E_1 = E$, $\nu_{32} = \nu$ and $G_{31} = G_{12} = G$, are chosen as reference quantities that are considered constants. Ratios

$$\beta = \frac{E_2}{E_1} = \frac{E_3}{E_1}, \tag{14}$$

$$\chi = \frac{\nu_{12}}{\nu_{32}} = \frac{\nu_{13}}{\nu_{32}} \tag{15}$$

and

$$\delta = \frac{G_{23}}{G_{31}} = \frac{G_{23}}{G_{12}} \ . \tag{16}$$

represent the remaining three, which may take values corresponding to materials ranging from isotropic to highly orthotropic. Solving of β, χ and δ for the fir and birch materials in Table 3, was done by taking the averages of the results of equations (14) - (16). The values $\beta = 0,059$, $\chi = 0,949$ and $\delta = 0,100$ were solved for fir. Birch has the following values: $\beta = 0,064$, $\chi = 0,629$ and $\delta = 0,240$. The values above are used later in Chapter 6, where the effects of the material properties are evaluated.

Simplifying the material model through the use of the six parameter model causes slight inaccuracy due to the fact that the ratios in equations (14), (15) and (16) are not exactly valid with wood. For instance, taking the average value of fir causes an absolute error in both of the values for the non-axial elastic moduli of 0,009. Given as a percentage of the average value of the ratios, it would equal to nearly 15,3 %. The same values for the

Poisson's ratios would be 0,205 % and 21,6 %. For the shear modulus, the following values were solved, 0,010 % and 9,82 %. The inaccuracy brought by these simplifications may be significant numerically, but considering the variations present in the properties of wood, the given values should be acceptable for use in the theoretical calculations presented in this thesis. However, the exact values used in practical applications should always be determined experimentally to account for variations in the structure of the wood as well as differing thermal and moisture properties.

2.3 Lay-up

In composite materials such as plywood, the lay-up of laminates is defined as the sequence of plies included in the laminate. Stacking sequences are written in terms of the angle α of each ply. For instance, for the plate in Figure 4 the orientations are denoted by [0/90/0/90/0], which indicates a laminate consisting of a ply with a 0 degree orientation, with the following ply being oriented at a 90 degree angle. Further plies follow the same logic, with adjacent plies always oriented perpendicular to each other. The plates evaluated in this thesis are symmetric laminates; this means that they have a sequence that is symmetric with respect to the geometric mid-plane. The geometric mid-plane also acts as the origin of the z-axis.

In traditional plywood plates, the number of layers is always odd, so that the uppermost and lowest layers are parallel as seen in Figure 4. A layer can consist of multiple plies, but the plies in a layer must always be parallel. Two adjacent layers in plywood are traditionally perpendicular and the outermost layers are placed so that the grain is parallel to the longer side of the plate so that the stacking sequence becomes for instance [0/90/0/90/0/90/0]. [Forest Products Laboratory, 2001, page 10-1]

Common parameters used with laminates are n indicating the number of plies in a laminate, t_i indicating the thickness of the plies and α_i indicating the orientation of the ply. The index i in the symbols signifies the number of the ply for which the parameter is defined. Numbering of plies begins from the lowest and increases towards the uppermost ply in the direction of the z-axis, with the first ply having the number 1. Plywood has usually a total thickness of more than 1,6 mm and less than 76 mm [Forest Products Laboratory, 2001,

page 10-1]. These values allow for the estimation of the total number of plies in a typical plywood plate to range from 3 to 47.

3 Plate model

3.1 Reissner-Mindlin Model

The Reissner-Mindlin plate model, which is a first-order shear deformation theory, provides a method for solving the displacement and stress in a plate. A plate is considered to be a solid body, which has two dimensions, for example width and length, that are significantly greater than the third dimension, which in this case would be thickness.

The Reissner-Mindlin model has a significant advantage over the Kirchoff plate model, which is a classical plate theory, in that it is capable of taking the transverse shear strains into account. The weakness of the Kirchoff model follows from the simplifications that lines normal to the mid-plane remain straight and normal in deformation. First-order shear deformation theories on the other hand are capable of taking into account the rotation of the transverse straight lines relative to the mid-plane normal so that they no longer need to be normal to the mid-plane after deformation. This advantage over classical plate theories has made the Reissner-Mindlin model and its derivatives the most common models used for solving the stresses and strains in plates. [Khandan et al., 2012] [Hughes, 2000, page 310]

3.2 Plate equations

The Reissner-Mindlin model is based on the following assumptions [Hughes, 2000, page 311].

1. The normal stress component in the direction of the z-axis vanishes, that is

$$\sigma_{zz} = 0. \tag{17}$$

2. The line segments that are originally normal to the reference plane remain straight in deformation

$$\begin{Bmatrix} u_x \\ u_y \\ u_z \end{Bmatrix} = \begin{Bmatrix} u(x,y) \\ v(x,y) \\ w(x,y) \end{Bmatrix} + z \begin{Bmatrix} \theta(x,y) \\ -\phi(x,y) \\ 0 \end{Bmatrix}. \tag{18}$$

In equation (18), the symbols u, v and w are the translation components of the line segments of assumption 2. in the directions of the x-, y- and z-axes respectively, while ϕ and θ are the rotation components of the line segments around the x- and y-axes of the plate, respectively.

The equilibrium equations for the Reissner-Mindlin model are those given by Smith [2005, page 356] with the addition of the external distributed moment c and the changing of the shear force symbols to Q.

$$\frac{\partial N_x}{\partial x} + \frac{\partial N_{yx}}{\partial y} + b_x = 0, \tag{19}$$

$$\frac{\partial N_y}{\partial y} + \frac{\partial N_{xy}}{\partial x} + b_y = 0, \tag{20}$$

$$\frac{\partial Q_x}{\partial x} + \frac{\partial Q_y}{\partial y} + b_z = 0, \tag{21}$$

$$\frac{\partial M_x}{\partial x} + \frac{\partial M_{yx}}{\partial y} - Q_x + c_x = 0, \tag{22}$$

$$\frac{\partial M_y}{\partial y} + \frac{\partial M_{xy}}{\partial x} - Q_y + c_y = 0, \tag{23}$$

where the symbols N, Q and M signify the normal force, shear force and moment resultants of the plate model. The terms b and c denote the external distributed forces and moments acting on the plate. In this thesis, the time dependency is neglected.

The distributed forces in equations (19) to (23) are, as given by Niu [1992, page 409],

$$\begin{Bmatrix} N_x \\ N_y \\ N_{xy} \end{Bmatrix} = \int \begin{Bmatrix} \sigma_x \\ \sigma_y \\ \sigma_{xy} \end{Bmatrix} dz, \tag{24}$$

$$\begin{Bmatrix} M_x \\ M_y \\ M_{xy} \end{Bmatrix} = \int z \begin{Bmatrix} \sigma_x \\ \sigma_y \\ \sigma_{xy} \end{Bmatrix} dz \tag{25}$$

and

$$\begin{Bmatrix} Q_y \\ Q_x \end{Bmatrix} = \int \begin{Bmatrix} \sigma_{yz} \\ \sigma_{zx} \end{Bmatrix} dz \ . \tag{26}$$

The integrals in equations (24) to (26) are taken over the thickness of the plate.

Equations (24) to (26) are needed to couple the external loads acting on a plate to the internal stresses and strains of the plate. These equations will be used in the following chapter to derive the constitutive equations for plywood, which can be used to solve the displacements and stresses acting in the different layers of a plate.

In addition to the relations of external loads to the internal stresses and strains in a plate, a set of boundary conditions is also needed for solving plate problems. Boundary conditions serve the purpose of providing known displacements and stresses to the edges of the plate that allow solutions to be found. The conditions are dependent of the plate attachments and can vary from clamped to totally free unconstrained edges. In this thesis, all of the edges are simply supported, which partially limits the rotations and displacements of the plate.

A plate that is simply supported cannot move in any direction at the points where the plate is attached to the supports. The only displacements that are allowed at these points are rotations around an axis aligned with the edge. Simply supported edges could be thought of as the edges of a plate placed on a triangular support with a cylindrical hinge at the point of contact. Using such a hinge would allow the plate to rotate as specified above and would simultaneously prevent the translational movements of the plate. A more precise explanation of the boundary conditions will be provided in Chapter 5, where a numerical calculation example for a simply supported plate will be given. [Reddy, 2004, page 247]

3.3 Constitutive equation for plywood

To calculate the stresses and strains in an externally loaded plate, a relationship between translations and rotations of the line segments and the stress resultants of the plate model is needed. This relation, which can be derived by using the constitutive equations of a ply in equations (8) and (9) and the definition of the stress resultants in equations (24) to (26).

By using the kinematic assumption in equation (18), the constitutive equation of a ply in equations (8) and (9) can be modified to provide the following form containing the translations and rotation components instead of the displacement components

$$\begin{Bmatrix} \sigma_x \\ \sigma_y \\ \sigma_{xy} \end{Bmatrix} = \begin{bmatrix} S_1 & S_3 & S_7 \\ S_3 & S_2 & S_8 \\ S_7 & S_8 & S_4 \end{bmatrix} \left(\begin{Bmatrix} \dfrac{\partial u}{\partial x} \\ \dfrac{\partial v}{\partial y} \\ \dfrac{\partial u}{\partial y} + \dfrac{\partial v}{\partial x} \end{Bmatrix} + z \begin{Bmatrix} \dfrac{\partial \theta}{\partial x} \\ -\dfrac{\partial \phi}{\partial y} \\ \dfrac{\partial \theta}{\partial y} - \dfrac{\partial \phi}{\partial x} \end{Bmatrix} \right) \tag{27}$$

and

$$\begin{Bmatrix} \sigma_{yz} \\ \sigma_{zx} \end{Bmatrix} = \begin{bmatrix} S_5 & S_9 \\ S_9 & S_6 \end{bmatrix} \begin{Bmatrix} \dfrac{\partial w}{\partial y} - \phi \\ \dfrac{\partial w}{\partial x} + \theta \end{Bmatrix} . \tag{28}$$

By substituting equations (27) and (28) into definitions (24) - (26), it is possible to write the following equations for the internal forces acting in the plate:

$$\begin{Bmatrix} N_x \\ N_y \\ N_{xy} \end{Bmatrix} = \mathbf{A} \begin{Bmatrix} \dfrac{\partial u}{\partial x} \\ \dfrac{\partial v}{\partial y} \\ \dfrac{\partial v}{\partial x} + \dfrac{\partial u}{\partial y} \end{Bmatrix} + \mathbf{C} \begin{Bmatrix} \dfrac{\partial \theta}{\partial x} \\ -\dfrac{\partial \phi}{\partial y} \\ \dfrac{\partial \theta}{\partial y} - \dfrac{\partial \phi}{\partial x} \end{Bmatrix} , \tag{29}$$

$$\begin{Bmatrix} M_x \\ M_y \\ M_{xy} \end{Bmatrix} = \mathbf{C}\begin{Bmatrix} \dfrac{\partial u}{\partial x} \\ \dfrac{\partial v}{\partial y} \\ \dfrac{\partial v}{\partial x}+\dfrac{\partial u}{\partial y} \end{Bmatrix} + \mathbf{B}\begin{Bmatrix} \dfrac{\partial \theta}{\partial x} \\ -\dfrac{\partial \phi}{\partial y} \\ \dfrac{\partial \theta}{\partial y}-\dfrac{\partial \phi}{\partial x} \end{Bmatrix} \tag{30}$$

and

$$\begin{Bmatrix} Q_y \\ Q_x \end{Bmatrix} = \mathbf{D}\begin{Bmatrix} \dfrac{\partial w}{\partial y}-\phi \\ \dfrac{\partial w}{\partial x}+\theta \end{Bmatrix}, \tag{31}$$

where

$$\mathbf{A} = \sum_{i=1}^{n} t_i \begin{bmatrix} S_1 & S_3 & S_7 \\ S_3 & S_2 & S_8 \\ S_7 & S_8 & S_4 \end{bmatrix}_i \tag{32}$$

signifies the translational relation between external forces and strains for the entire plate,

$$\mathbf{C} = \sum_{i=1}^{n} z_i t_i \begin{bmatrix} S_1 & S_3 & S_7 \\ S_3 & S_2 & S_8 \\ S_7 & S_8 & S_4 \end{bmatrix}_i \tag{33}$$

is the coupling between xy-planar forces and rotations around the x- and y-axes as well as xy-planar moments and translational displacements in the plate,

$$\mathbf{B} = \sum_{i=1}^{n} \left(z_i^{\,2} t_i + \frac{t_i^{\,3}}{12} \right) \begin{bmatrix} S_1 & S_3 & S_7 \\ S_3 & S_2 & S_8 \\ S_7 & S_8 & S_4 \end{bmatrix}_i \tag{34}$$

is the matrix that is used to define the relations between the xy-planar moments and the rotational displacements of the plate and

$$\mathbf{D} = \sum_{i=1}^{n} t_i \begin{bmatrix} S_5 & S_9 \\ S_9 & S_6 \end{bmatrix}_i \tag{35}$$

is used to connect the shear deformations to the shear forces acting inside the plate.

It should be noted at this point that if the laminate is symmetric, that is all plies that are located at opposite sides and equal distances from the mid-plane are identical in their properties and orientation, the $\mathbf{C}$ terms cancel each other and vanish. This means that there is no coupling between the linear and angular strains caused by the moments and normal forces acting on the plate. In practice, coupling would cause the plate to bend in xy-planar loading due to the differences in the stiffnesses of the plate.

3.4 Stress components

The equations that have been derived so far in this thesis can be used, for example, to solve the stresses acting at different z-axis locations in the plate. First, the elasticity matrix for the entire plate is solved by summing the elasticity matrices of the individual plies together through the use of equations (32) - (35). Equations (29) - (31) can then be used together with equilibrium equations (19) - (23) to solve the translation and rotation components of the plate at a given location on the z-axis of the plate. The solved translational and rotational components can then be inserted into the constitutive equations (27) and (28) to solve for the local stresses in the plate. The elasticity matrix to be used in the equations (27) and (28), is the one for the ply.

4 Two-scale plate theory

The Reissner-Mindlin model that has been discussed up to this point is capable of providing a quick and relatively accurate solution for most of the displacement and stress components of a plate problem. The major drawback of this model is the serious limitations of the model in the transverse shear and z-directional stress terms. As the Reissner-Mindlin model forces the normal stress in the z-axial direction to be negligible, the transverse shear and normal stress in the direction of the z-axis become a source of significant error.

In order to provide more accurate results without suffering significant penalties in terms of complexity or solving time, a new model has been developed by Freund [2016]. This model is based on the standard Reissner-Mindlin plate model, but incorporates significant improvements to the accuracy through the use of a warping displacement part that is added to the displacement assumption in equation (18) of the standard model.

The new two-scale plate model omits the kinetic assumption of the standard model and replaces the reduced elasticity matrix of equations (8) and (9) with the full three-dimensional elasticity matrix. The new kinematic assumption is of following form

$$\vec{u} = \vec{u}_0 + \Delta\vec{u} = \begin{Bmatrix} u_x \\ u_y \\ u_z \end{Bmatrix}^T \begin{Bmatrix} \vec{i} \\ \vec{j} \\ \vec{k} \end{Bmatrix} = \left(\begin{Bmatrix} u \\ v \\ w \end{Bmatrix} + z \begin{Bmatrix} \theta \\ -\phi \\ 0 \end{Bmatrix} + \begin{Bmatrix} \Delta u \\ \Delta v \\ \Delta w \end{Bmatrix} \right)^T \begin{Bmatrix} \vec{i} \\ \vec{j} \\ \vec{k} \end{Bmatrix}, \tag{36}$$

where the first term $\vec{u}_0$ is the kinematic assumption of the standard Reissner-Mindlin model, given in equation (18). The latter term, $\Delta\vec{u}$, is responsible of the straight line segments perpendicular to the mid-surface. In addition to the previous assumptions, the following assumption is also made [Freund, 2016]

$$\nabla\vec{u}=\begin{Bmatrix}\vec{i}\\ \vec{j}\\ \vec{k}\end{Bmatrix}^{T}\left(\begin{bmatrix}\frac{\partial u}{\partial x}+z\frac{\partial\theta}{\partial x} & \frac{\partial v}{\partial x}-z\frac{\partial\phi}{\partial x} & \frac{\partial w}{\partial x}\\ \frac{\partial u}{\partial y}+z\frac{\partial\theta}{\partial y} & \frac{\partial v}{\partial y}-z\frac{\partial\phi}{\partial y} & \frac{\partial w}{\partial y}\\ \theta & -\phi & 0\end{bmatrix}+\begin{bmatrix}0 & 0 & 0\\ 0 & 0 & 0\\ \frac{\partial\Delta u}{\partial z} & \frac{\partial\Delta v}{\partial z} & \frac{\partial\Delta w}{\partial z}\end{bmatrix}\right)\begin{Bmatrix}\vec{i}\\ \vec{j}\\ \vec{k}\end{Bmatrix}. \tag{37}$$

The equilibrium equations (19) - (23) and force resultant definitions (24) - (26) of the classical plate theory are preserved in the new model. The problem of finding the equations that correspond to the assumptions of the refined model can be obtained by beginning with the potential energy functional of 3D linear elasticity

$$\pi\left(\vec{u},\vec{\lambda}\right)=\frac{1}{2}\int_{\Omega}\int_{Z}\ddot{\sigma}_{c}:\nabla\vec{u}dzdA-\sum_{(i,j)\in J}\int_{\Omega}\int_{Z}\vec{\lambda}\cdot\Delta\vec{u}dzdA-$$

$$\int_{\Omega}\int_{Z}\vec{f}\cdot\vec{u}dzdA-\int_{\Omega}\int_{Z}\vec{t}\cdot\vec{u}dzds-\int_{\Omega}\sum_{\partial Z}\vec{q}\cdot\vec{u}dA\ , \tag{38}$$

where $\vec{\lambda}$ is the Lagrange multiplier of the same form as $\vec{u}_0$ and $\vec{f}$ is a given external volume force. Remaining terms $\vec{t}$ and $\vec{q}$ are the surface tractions acting on the plate's boundary surface and the upper and lower surface respectively. [Freund, 2016]

The following boundary value problem for the warping displacement has been given in [Freund, 2016]

$$\frac{\partial}{\partial z}\vec{\sigma}_i+\vec{f}+\vec{\lambda}=0\,,\ z\in\left]z_i-\frac{t_i}{2},z_i+\frac{t_i}{2}\right[\ ,\ i\in\{1,2,...,n\} \tag{39}$$

and

$$\int_{z_1-\frac{t_1}{2}}^{z_n+\frac{t_n}{2}}\delta\vec{\lambda}\cdot\Delta\vec{u}dz=0\,,\forall\delta\vec{\lambda}\,, \tag{40}$$

at the interface between two plies

$$\Delta\vec{u}_i(z_i+\frac{t_i}{2})-\Delta\vec{u}_{i+1}(z_{i+1}-\frac{t_{i+1}}{2})=0,\ i\in\{1,2,3,...,n-1\}, \tag{41}$$

$$\vec{\sigma}_i\left(z_i+\frac{t_i}{2}\right)-\vec{\sigma}_{i+1}\left(z_{i+1}-\frac{t_{i+1}}{2}\right)=0,\ i\in\{1,2,3,...,n-1\} \tag{42}$$

and at the outermost plies

$$\vec{\sigma}_1\left(z_1-\frac{t_1}{2}\right)=0\,, \tag{43}$$

$$\vec{\sigma}_n\left(z_n+\frac{t_n}{2}\right)-q=0\,. \tag{44}$$

In equations (39) to (44), $\vec{\lambda}$ represents the distributed volume force needed to enforce the orthogonality of the displacement parts, $\vec{f}$ is a given external volume force, $\Delta\vec{u}$ is the warping displacement, the subscript i signifies the ply number, z_i symbolizes the z-coordinate of the plies mid-plane, t_i is the symbol for the thickness of the ply, and the stress vector $\vec{\sigma}$ is defined as

$$\vec{\sigma}=\vec{k}\cdot\vec{\sigma}\,. \tag{45}$$

Equations (41) and (42) enforce the displacements and tractions of the plate to be continuous over the interfaces of two plies. The boundary value problems can be used to solve the warping displacement when the stress expression

$$\vec{\sigma}=\vec{\vec{E}}:\left(\nabla\vec{u}_0+\vec{k}\frac{\partial}{\partial z}\Delta\vec{u}\right) \tag{46}$$

is substituted into equations there. [Freund, 2016]

Once the warping displacement is known, the plate equations can be used to solve the displacements and rotations of the plate in a similar manner as those of the standard model. [Freund, 2016]

First, warping displacements are substituted in equation (37) to get the displacement gradient in terms of the strain measures of the standard plate model. Second, equations (8) and (9) give the stress components in terms of the strain measures seen in equations (5) and (6). The remaining task is to use the stress resultant definitions in equations (24) - (26) to

calculate the $\mathbf{A}$, $\mathbf{B}$, $\mathbf{C}$ and $\mathbf{D}$ terms of equations (29) - (35). It is noteworthy that the kinetic assumption of the standard plate model is omitted in equations (8) and (9). The final step that remains, is using the equilibrium equations (19) to (23) with equations (24) to (26) and (29) to (31) to solve for the translation and rotation components of the plate model.

5 Model problem and methods of solution

5.1 Rectangular plate problem

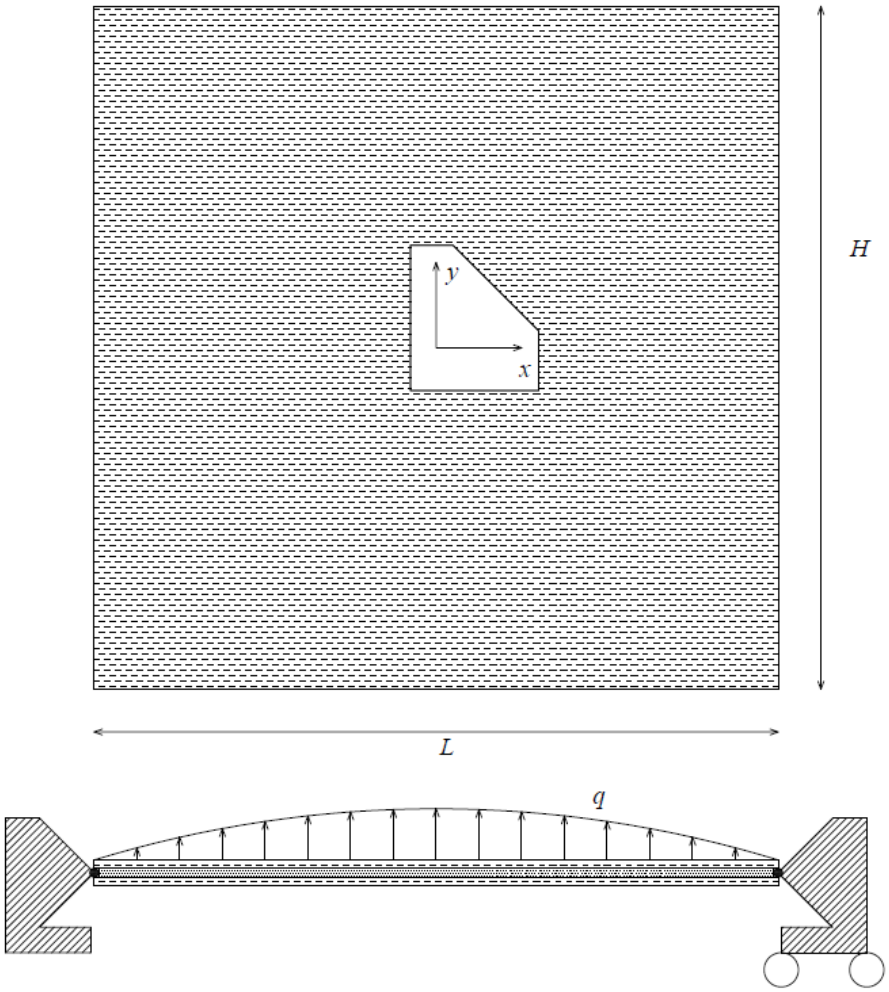

Figure 5. Plate loading and edge support.

The new refined model described in the previous chapter will be compared with the solution provided by the standard model and an exact solution for rectangular bidirectional composite plates. This thesis will use the solution derived by N. J. Pagano [1969] as the baseline exact solution of the evaluations.

The comparison of the models will be done using a rectangular plate that is loaded by sinusoidal traction acting on the upper surface. The plates are simply supported from their

edges, with the right and upper edges of the plate allowing planar translation. An illustration of the plate attachment and loading is shown in Figure 5.

Having simply supported edges means that no vertical displacements are allowed at the edges, nor is any rotation around the y-axis allowed at the edges that are parallel to the x-axis or rotation around the x-axis allowed at the edges that are parallel to the y-axis. The normal forces acting in the direction of the edge as well as the moments acting around the edge are also assumed to be zero at the edge.

The plate is loaded by normal traction acting on the upper surface, while the lower surface is traction-free. The applied distributed force [Pagano, 1969] acts on the entire surface in its normal direction and has a magnitude of

$$q(x,y) = q_0 \sin\left(\frac{\pi x}{L}\right) \sin\left(\frac{\pi y}{H}\right). \tag{47}$$

All of the plate model solutions are of the following form

$$u_x = U(z) \cos\left(\frac{\pi x}{L}\right) \sin\left(\frac{\pi y}{H}\right), \tag{48}$$

$$u_y = V(z) \sin\left(\frac{\pi x}{L}\right) \cos\left(\frac{\pi y}{H}\right) \tag{49}$$

and

$$u_z = W(z) \sin\left(\frac{\pi x}{L}\right) \sin\left(\frac{\pi y}{H}\right). \tag{50}$$

The solutions also require the following assumptions to be made. The displacements are continuous over the thickness of the plate, that is, there is no sliding allowed between the plies. The stresses acting on an area element with a normal in the z-direction are also continuous over the thickness of the plate, that is, there are no jumps in the magnitude of the non-xy-planar stresses at the interfaces of two plies. The external traction acts on the whole plate and is sinusoidal. The lay-ups that are used are symmetric, which means that

the number of plies is always odd and that the top and bottom plies are always oriented in the same direction.

As all of the solutions are of the same form, the differences between the models follow from the differences in $U(z)$, $V(z)$ and $W(z)$.

The next chapters will describe how the models are used to find the displacement and stress in a plate, beginning with the standard Reissner-Mindlin model and ending with Pagano's exact solution. Included in the chapter on the exact solution is also a brief description of the model and the assumptions included in it.

5.2 Standard model

The standard model solution used in the comparisons of this chapter is based on the equations provided in Chapter 3.3. The solution begins with the assumption of the exact solutions of the forms

$$w = a_1 \sin\left(\frac{\pi x}{L}\right)\sin\left(\frac{\pi y}{H}\right), \tag{51}$$

$$\phi = a_2 \sin\left(\frac{\pi x}{L}\right)\cos\left(\frac{\pi y}{H}\right)$$

and (52)

$$\theta = a_3 \cos\left(\frac{\pi x}{L}\right)\sin\left(\frac{\pi y}{H}\right). \tag{53}$$

Expressions (51) to (53) can then be substituted into equation (18), with the translational displacement components u and v being zeros, as there are no external x- and y-directional forces acting on the plate.

Substituting equations (51) - (53) into equation (18) yields

$$u_x = a_3 z \cos\left(\frac{\pi x}{L}\right)\sin\left(\frac{\pi y}{H}\right), \tag{54}$$

$$u_y = a_2 z \sin\left(\frac{\pi x}{L}\right)\cos\left(\frac{\pi y}{H}\right) \tag{55}$$

and

$$u_z = a_1 \sin\left(\frac{\pi x}{L}\right)\sin\left(\frac{\pi y}{H}\right). \tag{56}$$

The results show that the solutions of the standard model correspond to the equations in (48).

The solving of the unknown constants in the displacement solutions requires the constitutive equations for plywood of equations (19) to (23), using the equations (29), (30), (32) and (34) of Chapter 3.3. As the laminate is symmetric, the **C** terms vanish from the equations, leaving only the **A**, **B** and **D** terms into the constitutive equation.

In practice, the principle of minimum potential energy is used to find the values of the unknown coefficients of equations (51) to (53). Chapter 3.3 contains the necessary equations and definitions that are needed for the following equations (57) to (59). Potential energy of internal forces

$$U_{\text{int}} = \frac{1}{2}\int_0^H\int_0^L \begin{Bmatrix} M_x \\ M_y \\ M_{xy} \end{Bmatrix}^T \begin{Bmatrix} \theta_{,x} \\ -\phi_{,y} \\ \theta_{,y} - \phi_{,x} \end{Bmatrix} + \begin{Bmatrix} Q_x \\ Q_y \end{Bmatrix}^T \begin{Bmatrix} w_{,y} - \phi \\ w_{,x} + \theta \end{Bmatrix} dx\, dy\,. \tag{57}$$

depends on the stress resultants of the plate model and their work conjugate strain components expressed in terms of the translation and rotation components.

Work by external forces is calculated by integrating the external distributed force multiplied by the displacement in the direction of the z-axis over the plate's area as follows

$$W_{\text{ext}} = \int_0^H\int_0^L q\, w\, dx\, dy\ . \tag{58}$$

The external work (58) is subtracted from the internal potential energy (57) to provide the total potential level of the plate U

$$U = U_{\text{int}} - W_{\text{ext}} \ . \tag{59}$$

When the expressions in equations (51) - (53) are substituted into equation (59), the resulting potential energy function will only contain the unknowns a_1, a_2 and a_3. The function is then minimized to find the unknown values of a_1, a_2 and a_3 of equations (51)-(53).

The resulting values are then substituted back into the displacement equations (51) to (53) that are needed in equations (27) and (28) to find the stress acting in each of the plies. The S terms of the equations have been defined in appendix A.2.

5.3 Refined model

Calculation of the displacement and stress using the refined model begins with finding the warping displacements using the boundary value problem of equations (39) to (44). Once the warping displacement is known, they can be substituted in equation (37) to get the displacement gradient in terms of the strain measures of the standard model. Then, equations (8) and (9) are used to obtain the stress components in terms of the strain measures in each ply.

The stress components can then be used with the stress resultant definitions of equations (24) to (26) to obtain the $\mathbf{A}$, $\mathbf{B}$, $\mathbf{C}$ and $\mathbf{D}$ terms from the equations (29) to (35). The last part is to use the equilibrium equations (19) to (23) with equations (24) to (26) and (29) to (31) to solve for the translation and rotation components of the plate model. From here on, the rest of the solution proceeds with the same procedure as the standard model of Chapter 5.2.

In practice, the solutions used in the comparison were calculated using the method described above. To hasten the comparisons and to provide graphical representations of the results, a Mathematica code was used to perform the numerical work.

5.4 Pagano's method

In his article, Pagano [1969] describes a three-dimensional elasticity solution that can be used to find the displacement and stress according to the full 3 dimensional linear elasticity theory, considered here as the precise theory. In this method, the laminate response is defined by the solution of a boundary value problem given by the linear elasticity theory within each layer, the boundary conditions defined for the plate and the interface continuity conditions at the interfaces of the layers. The interface continuity conditions serve the purpose of fixing the layers together so that particles that are located adjacent to each other in an unloaded state remain adjacent to each other in loading. This is done because the plies are laminated together, meaning that they cannot slide relative to each other. The importance for this condition can be exemplified with the difference in the properties between a plate with layers that are glued together and a plate with layers simply stacked on top of each other without the glue. The plate where the layers can slide in relation to each other deforms in a different manner than the one where the layers are fixed together. The boundary conditions of the plate were discussed in Chapter 5.1 and will not be repeated here.

The solution is given for a plate with properties, loads and constraints as described in Chapter 5.1. Pagano provides the same constitutive equations for any layer in the plate as those shown in equations (5) and (6). The model assumes a cross-stacked structure, that is, all of the layers are oriented either at 0 degrees or 90 degrees and the laminate is symmetric. This causes the components S_7, S_8 and S_{13} to be 0 in the equations given in appendix A.2.

The governing field equations of the plate are given in terms of the displacement components as follows [Pagano, 1969]

$$S_1 u_{x,xx} + S_4 u_{x,yy} + S_6 u_{x,zz} + (S_3 + S_4) u_{y,xy} + (S_{11} + S_6) u_{z,xz} = 0 \ , \tag{60}$$

$$(S_3 + S_4) u_{x,xy} + S_4 u_{y,xx} + S_2 u_{y,yy} + S_5 u_{y,zz} + (S_{12} + S_5) u_{z,yz} = 0 \tag{61}$$

and

$$\left(S_{11}+S_6\right)u_{x,xz}+\left(S_{12}+S_5\right)u_{y,yz}+S_6u_{z,xx}+S_5u_{z,yy}+S_{10}u_{z,zz}=0\,. \tag{62}$$

The S-terms are given in appendix A.2. By substituting the equations into equations (60) to (62) the outcome is the ordinary differential equations

$$\left(-\frac{\pi^2}{L^2}S_1-\frac{\pi^2}{H^2}S_4\right)U+S_6U''-\left(S_3+S_4\right)V\frac{\pi^2}{LH}+\left(S_{11}+S_6\right)W'\frac{\pi}{L}=0\,, \tag{63}$$

$$-\left(S_3+S_4\right)U\frac{\pi^2}{LH}-\left(S_4\frac{\pi^2}{L^2}+\frac{\pi^2}{H^2}S_2\right)V+S_5V''+\left(S_{12}+S_5\right)W'\frac{\pi}{H}=0 \tag{64}$$

and

$$-\left(S_{11}+S_6\right)U'\frac{\pi}{L}-\left(S_{12}+S_5\right)V'\frac{\pi}{H}-\left(S_6\frac{\pi^2}{L^2}+\frac{\pi^2}{H^2}S_5\right)W+S_{10}W''=0 \tag{65}$$

for U, V and W.

In equations (63) - (65), derivation of a function with respect to z is symbolized with the Lagrange's notation's $'$ prime mark. The derivations done on each row cause the sine and cosine terms of each of the displacement component to become identical. As each of the components have the same multiplier, the multiplier can be left out of the solution, as it no longer has any effect on the solution.

After solving the equations of U, V and W, the upper and lower surface conditions should be defined for the plate. This condition states that the lower surface is stress-free in the z-direction, while the upper surface is only stressed by the distributed force, defined in equation (47), in the z-direction. This can be written as

$$\vec{\sigma}_1\left(z_1-\frac{t_1}{2}\right)-q=0\,, \tag{66}$$

$$\vec{\sigma}_n\left(z_n+\frac{t_n}{2}\right)=0\,, \tag{67}$$

in which z_i is the z-coordinate of the ply's mid-plane, t_i is the thickness of the ply and q is the external surface force acting on the ply.

The next step is defining the interface condition, where the displacements at opposing ply surfaces are set to be equal. This can be done by defining, for instance,

$$U_i(z_i + \frac{t_i}{2}) - U_{i+1}(z_{i+1} - \frac{t_{i+1}}{2}) = 0,\ i \in \{1,2,...,n-1\}, \tag{68}$$

$$V_i(z_i + \frac{t_i}{2}) - V_{i+1}(z_{i+1} - \frac{t_{i+1}}{2}) = 0,\ i \in \{1,2,...,n-1\} \tag{69}$$

and

$$W_i(z_i + \frac{t_i}{2}) - W_{i+1}(z_{i+1} - \frac{t_{i+1}}{2}) = 0,\ i \in \{1,2,...,n-1\}. \tag{70}$$

This is followed by defining the z-directional stresses to be equal on both sides of the interface points, that is, the condition is that the z-directional stress components remain continuous. This can be done by defining

$$\vec{\sigma}_i\left(z_i + \frac{t_i}{2}\right) - \vec{\sigma}_{i+1}\left(z_{i+1} - \frac{t_{i+1}}{2}\right) = 0,\ i \in \{1,2,...,n-1\}. \tag{71}$$

These conditions are then substituted into equation (5) and (6), where the values of U, V and W have been substituted. This set of equations can then be calculated for the different values of the stiffness matrix $\mathbf{S}$. After the values of $\mathbf{S}$ have been found, the results can be substituted into equations (5) and (6) to provide the values of the stresses and displacements in the different directions.

In practice, Pagano's method is used as follows. First the equilibrium equations (60) - (62) providing three ordinary differential equations for the unknown variables U, V and W are derived. Solving the differential equations provides the values of the variables, which are then substituted into the equations for the strains and stresses given in equations (48), (18), (5) and (6). At this point, the resulting equations end up with similar sine and cosine multipliers as the previous models, which can therefore be left out from further evaluation,

as they have no effect on the relative accuracy of the model. After the removal of the multipliers is done, the surface and interface conditions are defined and used to find the values of the remaining unknown S_{ij} terms. Once these steps have been taken, it is possible to substitute all of the values to the equations of the strains and stresses defined earlier to provide the desired values. Practical calculations used in the evaluation are done using a Mathematica code, which provides the solutions of each of the three models rapidly and easily. This solution is also justifiable, as it provides an easy and accurate method of calculating the L_2 norms and drawing each model's solution into the same graphs.

It was found that all of the equations given by the different models used for the evaluation of the refined model included the same sine and cosine terms as multipliers, which allowed these terms to be omitted from the solution. This omission is justifiable as multiplying two variables by the same multiplier does not affect the ratio between the two variables. The significance of this omission is that the following comparison of accuracies is valid at any point on the xy-plane of the plate as the omitted terms are the only parts of the equations containing x- and y-coordinates. The omitted terms follow from the elasticity solutions of the plate (48) that satisfy the edge conditions of a simply supported plate. These same elasticity solutions are used in all of the three evaluated models and provide the same sine and cosine multipliers to the end results and therefore have no effect on the accuracies of the different models.

6 Comparison of the models

The goal for this chapter is to determine when it is suitable to use the refined model [Freund, 2016] and what its accuracy is when it is compared to the exact solution [Pagano, 1969]. The parameters that are going to be varied in this evaluation are the number of plies, the aspect ratio of the plate as well as the ratio of thickness against the length of the plate. The effect the material type has on the results is also evaluated by comparing the accuracies of the model for a material that is isotropic and two materials that are orthotropic.

Due to the availability of an exact solution, the case that will be evaluated is fixed in terms of the loading and boundary conditions. The next Chapter 6.1 will describe the case and the boundary conditions used in the solution.

6.1 Plate parameters

As the focus of this thesis is on plywood plates, the plates used for the majority of comparisons will have lay-ups and material properties that are typical to plywood. An isotropic material will also be used to evaluate the effect of orthotropy on the accuracy of the models.

The plate will have a 0/90 degree lay-up, with odd layers having a 0 degree orientation and even layers a 90 degree orientation. The dimensions of the plate depend on the case as is shown in Tables 4 and 5.

Table 4. Constant plate parameters.

Plate length L	Modulus of elasticity E	Shear modulus G	Poisson's ratio ν_{32}	Loading ratio μ	Ply thickness t_i
1	1	1	1/3	1/10	t/n

Table 5. Varied plate parameters.

Case	Number of plies n	Aspect ratio γ	Thickness ratio η	Material (β, χ, δ)
1	Variable (3 - 99)	1	1/20	Orthotropic $\beta = 0{,}01$ $\chi = 0{,}1$ $\delta = 0{,}01$
2	3	Variable (1 – 2000)	1/20	Orthotropic $\beta = 0{,}01$ $\chi = 0{,}1$ $\delta = 0{,}01$
3	3	1	Variable (0,004– 0,3)	Orthotropic $\beta = 0{,}01$ $\chi = 0{,}1$ $\delta = 0{,}01$
4	3	1	1/20	Fir $\beta = 0{,}059$ $\chi = 0{,}949$ $\delta = 0{,}100$
5	3	1	1/20	Isotropic $\beta = 1$ $\chi = 1$ $\delta = 1$

To allow the evaluation of the model's accuracy for plywood, the material properties of case 4 are chosen so that they provide a reasonably good approximation of the properties of typical plywood. Therefore the properties presented in Table 3 of Chapter 2.2 for fir are used in case 4. For the extremely orthotropic cases 1 - 3, values with exaggerated orthotropy are chosen. In the isotropic case 5, the properties of steel given in Table 3 are used.

The ranges of the variables were chosen as follows. The number of plies was limited to the range of 3 to 99, as this range can be seen in plywood, with higher values being less common. The aspect ratio, defined as the ratio between the width and length of the plate, was limited to the range of 1 to 2000. Thickness ratio is defined as the ratio of the thickness divided by the length of the plate. The range of the thickness ratio that was examined in this thesis, was limited to the range of 0,004 to 0,3.

6.2 Results

This chapter contains the results and comparisons for all of the displacement and stress components of the different models. The results for the different cases given by the three different models discussed in this thesis are shown in the following graphs as functions of the z-coordinate. As the results for each of the three models are plotted into the same graph, the comparison of the results becomes significantly easier, as it is possible to quickly see how well the refined model [Freund, 2016] compares to the exact solution provided by Pagano [1969] and the standard model. The colors used in the graphs are as follows: red is for the standard model, blue is for Pagano's model and black is for the refined model.

The accuracy of the models is analyzed by calculating the error in the standard and refined plate model solutions' displacement and stress components. The error measure is as follows

$$\|a-b\| = \frac{\sqrt{\int (a-b)^2 \, dz}}{\sqrt{\int b^2 dz}}, \tag{72}$$

in which a represents the displacement or stress component of the standard or refined model and b the corresponding exact result from Pagano's solution. The integrals are taken over the thickness of the entire plate. Due to the form of the equation, the results are given as the ratio of the difference between a model and the exact result to the exact result and can be converted to percents by multiplying by 100.

The values of the error are given with an accuracy of two decimals, as higher accuracies may already begin to suffer from the inaccuracies of the solver. These kinds of errors may follow from rounding and approximations done by the program that is used to solve the different components.

6.2.1 Case 1, effect of numbers of plies

Case 1 shows the effect of the number of plies, n, for a highly anisotropic layer material. In the first case, the length of the plate, L, the modulus of elasticity, E, and the shear modulus, G, are set to be 1. In addition, ply thickness t_i is defined as t/n, loading ratio as $\mu = 1/10$ and Poisson's ratio as $\nu_{32} = 1/3$. The parameters that are given a fixed value in case 1 are the aspect ratio, $\gamma = H/L = 1$, thickness ratio, $\eta = t/L = 1/20$, and material property ratios: $\beta = E_2/E_1 = E_3/E_1 = 0{,}01$, $\chi = \nu_{12}/\nu_{32} = \nu_{13}/\nu_{32} = 0{,}1$ and $\delta = G_{23}/G_{31} = G_{23}/G_{12} = 0{,}01$. Case 1 evaluates the effect of the number of plies by varying the number of plies, n, from 3 to 99 plies.

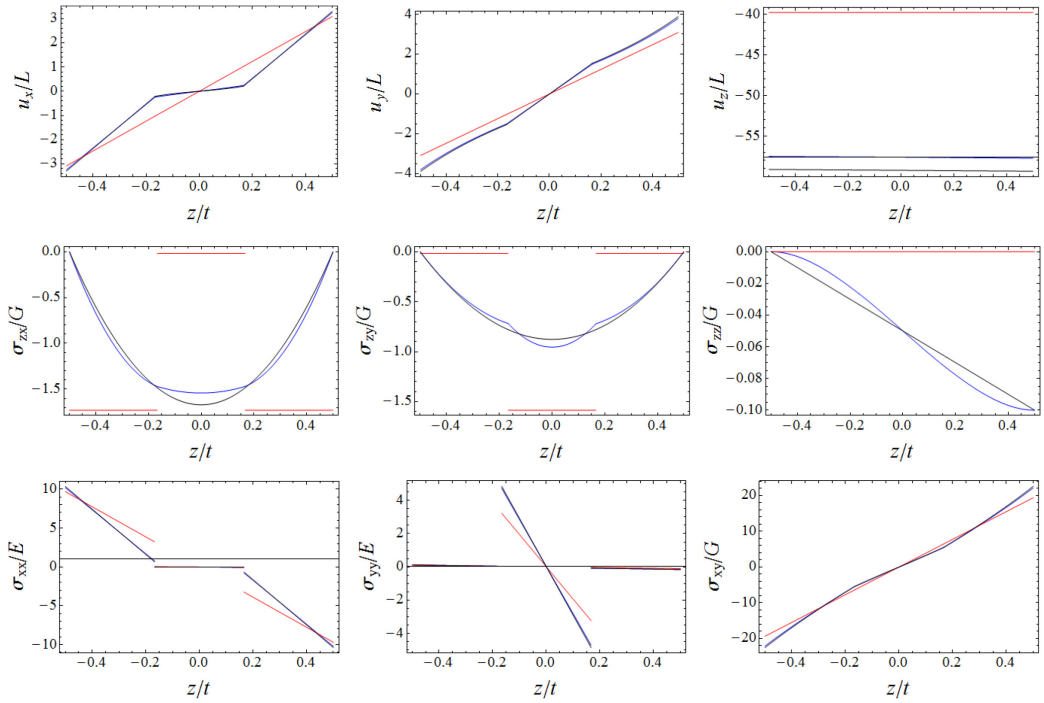

Figure 6. Displacement and stress components for a 3 ply orthotropic plate. Red curves are for the standard model, blue for Pagano's model and black for the refined model.

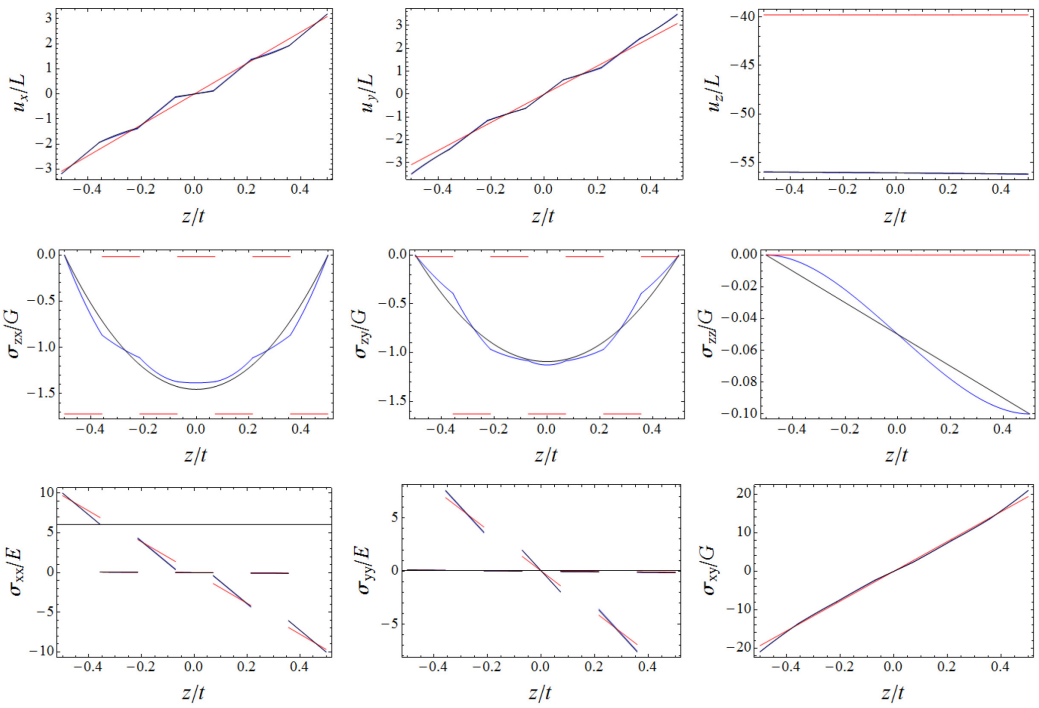

Figure 7. Displacement and stress components for a 7 ply orthotropic plate. Red curves are for the standard model, blue for Pagano's model and black for the refined model.

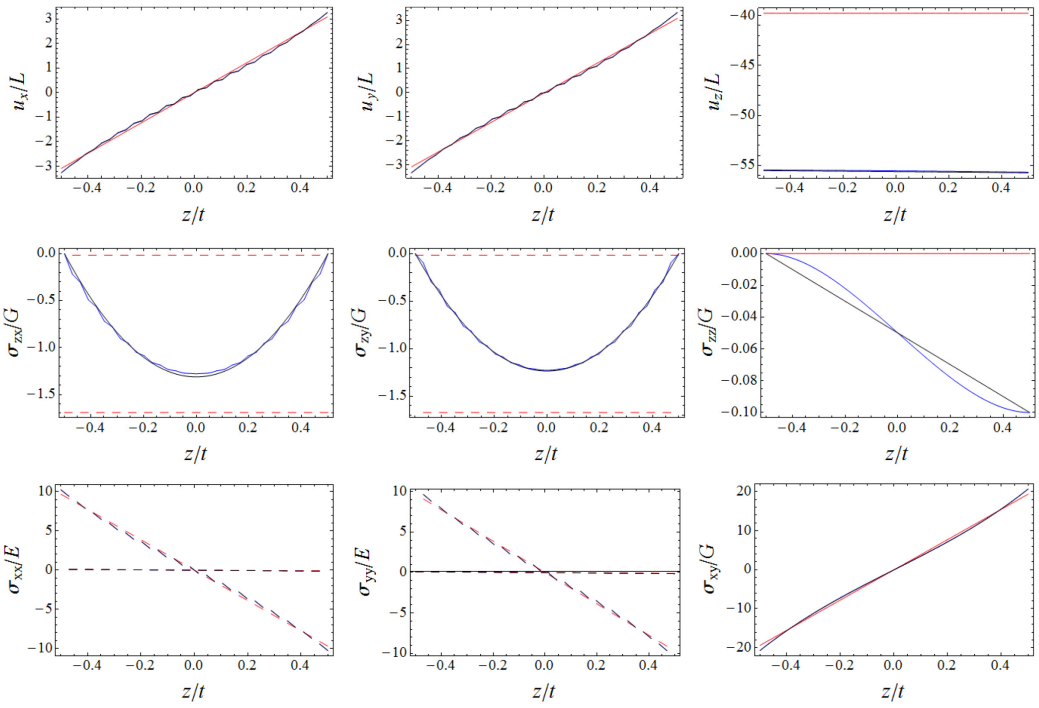

Figure 8. Displacement and stress components for a 33 ply orthotropic plate. Red curves are for the standard model, blue for Pagano's model and black for the refined model.

Table 6. Error in the displacement components.

	Refined model			Standard model		
Number of plies n	u_x	u_y	u_z	u_x	u_y	u_z
3	0,02	0,02	0,03	0,27	0,20	0,31
5	0,01	0,02	0,00	0,13	0,13	0,30
7	0,01	0,01	0,00	0,09	0,09	0,29
11	0,01	0,01	0,00	0,07	0,07	0,29
33	0,00	0,00	0,00	0,05	0,05	0,28
99	0,00	0,00	0,00	0,04	0,04	0,28

Table 7. Error in the continuous stress components.

	Refined model			Standard model		
Number of plies n	σ_{zx}	σ_{zy}	σ_{zz}	σ_{zx}	σ_{zy}	σ_{zz}
3	0,06	0,06	0,11	0,95	0,87	1
5	0,08	0,10	0,11	0,98	0,94	1
7	0,07	0,08	0,11	0,98	0,96	1
11	0,06	0,05	0,11	0,99	0,97	1
33	0,03	0,02	0,11	0,99	0,98	1
99	0,02	0,01	0,11	0,98	0,98	1

Table 8. Error in the discontinuous stress components.

	Refined model			Standard model		
Number of plies n	σ_{xx}	σ_{yy}	σ_{xy}	σ_{xx}	σ_{yy}	σ_{xy}
3	0,01	0,03	0,02	0,21	0,31	0,09
5	0,00	0,03	0,01	0,11	0,12	0,06
7	0,01	0,02	0,00	0,08	0,07	0,05
11	0,01	0,01	0,00	0,06	0,05	0,04
33	0,00	0,00	0,00	0,05	0,04	0,04
99	0,00	0,00	0,00	0,05	0,04	0,04

Table 6 shows, that the refined model's accuracy for the x- and y-directional displacements improves as the number of plies increases. The accuracy of the refined model is notably better than that of the standard model for all of the displacement components. The refined model's z-directional displacement component's accuracy improves in the number of plies, but suffers a slight decrease in accuracy at approximately 33 plies. This decrease is insignificant enough to vanish when the result is rounded to two decimals, which may indicate that the reduction in accuracy is caused by numerical error. Still, using the refined model is significantly more accurate for this component than the standard model for any number of plies.

Tables 7 and 8 show that the refined model is far more accurate in the solutions of the stress components σ_{xx}, σ_{yy}, σ_{xy}, σ_{zx}, σ_{zy} and σ_{zz} than the standard model for any number of plies. The accuracy of the refined model weakens slightly at 5 plies but continues to improve at higher numbers. The accuracy of σ_{zz} settles to 0,110 and the number of plies seems to have little to no effect on the accuracy of this component. Although this is quite a lot more error when compared to the other components, this is still a major improvement over the standard model, which is unable to provide a value for this stress.

It is important to note that the refined model also provides significantly improved distributions of the stresses and strains compared to the results of the standard model. This is especially highlighted with the z-directional shear stresses, where the standard model provides a discontinuous form, which would not be physically possible in a continuous laminate. The forms of the distributions are illustrated in Figures 6 - 8.

The improved accuracy of the refined model is such that it is recommended to use the refined model for all numbers of plies. The other reason for the recommendation is in the time it takes to derive the solutions. The refined model is able to solve the stresses and strains in a plate significantly faster than the exact solution, something that is highlighted even further with increasing numbers of plies.

6.2.2 Case 2, effect of aspect ratio

Case 2 evaluates the effect of the aspect ratio for a highly anisotropic layer material by varying the ratio, $\gamma = H / L$, from 1 to 2000. Values that are less than 1 for the aspect ratio are not evaluated, as the relative thickness t / L becomes greater when the plate becomes shorter than 1. In the second case, the length of the plate, L, the modulus of elasticity, E, and the shear modulus, G, are set to be 1. In addition, ply thickness t_i is defined as t / n, loading ratio as $\mu = 1/10$ and Poisson's ratio as $\nu_{32} = 1/3$. The parameters that are given a fixed value in case 2 are; number of plies, $n = 3$, thickness ratio, $\eta = t / L = 1/20$ and material property ratios: $\beta = E_2 / E_1 = E_3 / E_1 = 0{,}01$, $\chi = \nu_{12} / \nu_{32} = \nu_{13} / \nu_{32} = 0{,}1$ and $\delta = G_{23} / G_{31} = G_{23} / G_{12} = 0{,}01$.

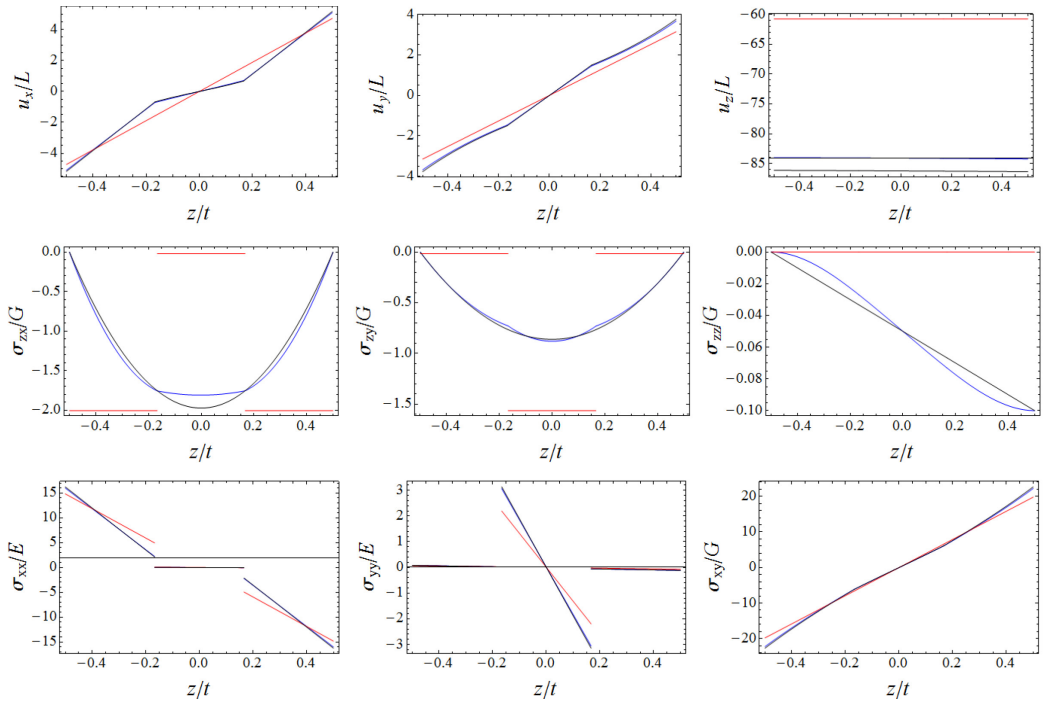

Figure 9. Displacement and stress components for an orthotropic plate with an aspect ratio of 1,5. Red curves are for the standard model, blue for Pagano's model and black for the refined model.

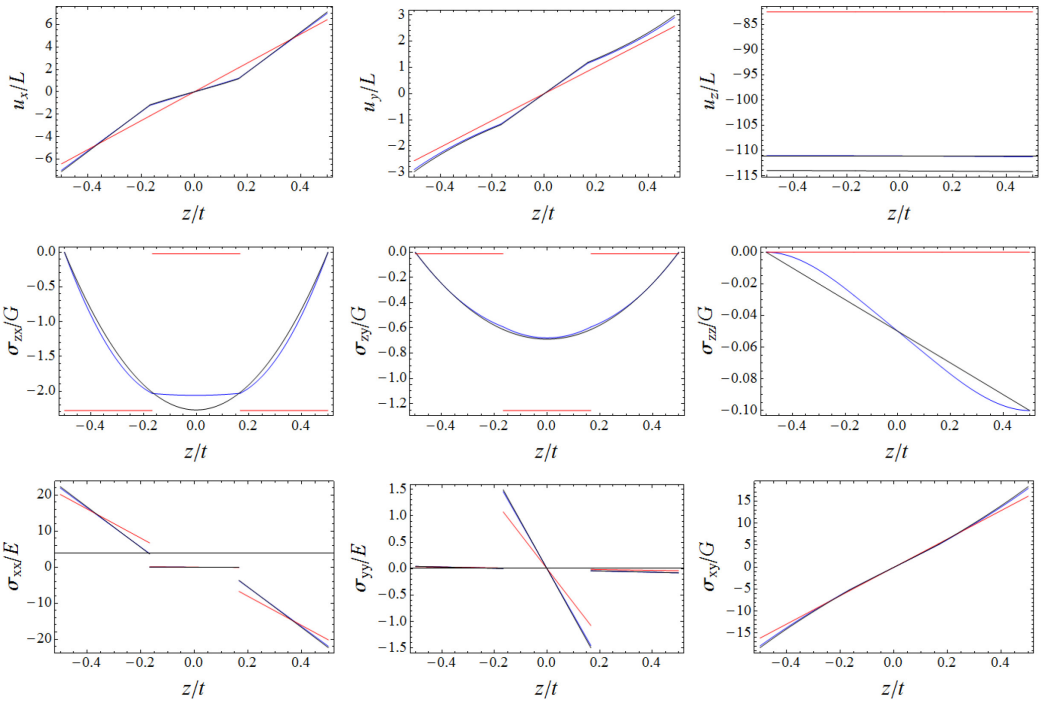

Figure 10. Displacement and stress components for an orthotropic plate with an aspect ratio of 2,5. Red curves are for the standard model, blue for Pagano's model and black for the refined model.

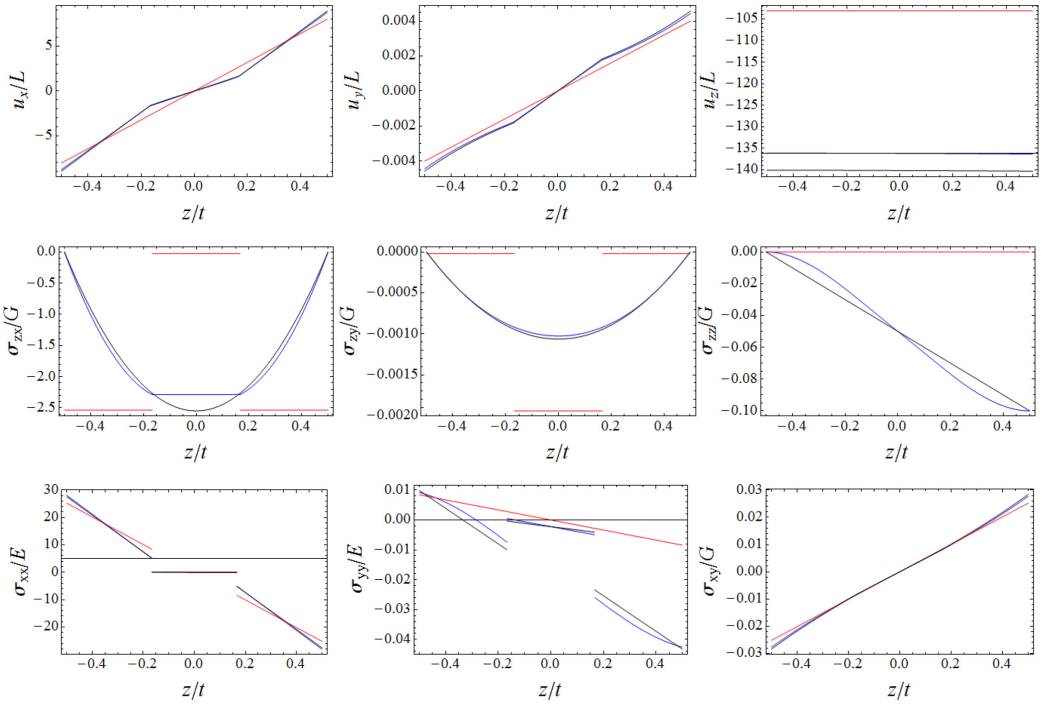

Figure 11. Displacement and stress components for an orthotropic plate with an aspect ratio of 2000. Red curves are for the standard model, blue for Pagano's model and black for the refined model.

Table 9. Error in the displacement components.

	Refined model			Standard model		
Aspect ratio γ	u_x	u_y	u_z	u_x	u_y	u_z
1	0,02	0,02	0,03	0,27	0,20	0,31
1,5	0,01	0,03	0,03	0,18	0,16	0,28
2	0,02	0,03	0,03	0,15	0,14	0,26
2,5	0,02	0,03	0,03	0,14	0,13	0,26
20	0,02	0,03	0,03	0,12	0,12	0,24
200	0,02	0,03	0,03	0,12	0,12	0,24
2000	0,02	0,03	0,03	0,12	0,12	0,24

Table 10. Error in the continuous stress components.

	Refined model			Standard model		
Aspect ratio γ	σ_{zx}	σ_{zy}	σ_{zz}	σ_{zx}	σ_{zy}	σ_{zz}
1	0,06	0,06	0,11	0,95	0,87	1
1,5	0,06	0,03	0,10	0,94	0,92	1
2	0,06	0,02	0,10	0,93	0,94	1
2,5	0,07	0,02	0,10	0,93	0,95	1
20	0,07	0,03	0,10	0,92	0,96	1
200	0,07	0,03	0,10	0,92	0,96	1
2000	0,07	0,03	0,10	0,92	0,96	1

Table 11. Error in the discontinuous stress components.

	Refined model			Standard model		
Aspect ratio γ	σ_{xx}	σ_{yy}	σ_{xy}	σ_{xx}	σ_{yy}	σ_{xy}
1	0,01	0,03	0,02	0,21	0,31	0,09
1,5	0,01	0,03	0,02	0,14	0,28	0,07
2	0,01	0,03	0,02	0,12	0,27	0,07
2,5	0,01	0,03	0,02	0,11	0,26	0,06
20	0,02	0,08	0,02	0,09	0,76	0,06
200	0,02	0,09	0,02	0,09	0,84	0,06
2000	0,02	0,09	0,02	0,09	0,84	0,06

The results in Tables 9 to 11 show that the refined model is superior in terms of accuracy to the standard model at all aspect ratios for nearly all of the compared variables.

The y-directional displacement component of the refined model becomes less accurate with increasing aspect ratios. Conversely, the x- and z-directional displacement components retain their accuracies after a brief improvement at low ratios. Still, it is seen that the increase in inaccuracy is very slow and that these components remain significantly more accurate than the standard model for all aspect ratios.

As the aspect ratio of the plate becomes greater, the accuracy of the y-directional shear stress component σ_{zy} improves. Conversely, the accuracy of the x-directional shear stress component σ_{zx} becomes less accurate at increasing aspect ratios. The accuracy of the z-directional stress seems to settle towards 0,100.

The normal stresses in the x- and y-axis directions as well as the shear stress in the xy-direction become less accurate with increasing aspect ratios. There is a slight jump in inaccuracy at an aspect ratio of 1, where the accuracy is less than in the immediate vicinity of this value.

It is important to note that the refined model provides significantly improved distributions of the stresses and strains compared to the results of the standard model. This is especially highlighted with the z-directional shear stresses, where the standard model provides a discontinuous form, which would not be physically possible in a continuous laminate. The form of the refined model's z-directional shear stress distributions are less accurate with aspect ratios below 1. The forms of the distributions are illustrated in Figures 9 - 11.

6.2.3 Case 3, effect of thickness ratio

Case 3 evaluates the effect of the thickness ratio by varying the ratio, $\eta = t / L$, from 0,004 to 0,3. In the third case, the length of the plate, L, the modulus of elasticity, E, and the shear modulus, G, are set to be 1. In addition, ply thickness t_i is defined as t / n, loading ratio as $\mu = 1/10$ and Poisson's ratio as $\nu_{32} = 1/3$. The parameters that are given a fixed value in case 3 are: number of plies, $n = 3$, aspect ratio, $\gamma = H / L = 1$ and material property ratios, $\beta = E_2 / E_1 = E_3 / E_1 = 0,01$, $\chi = \nu_{12} / \nu_{32} = \nu_{13} / \nu_{32} = 0,1$ and $\delta = G_{23} / G_{31} = G_{23} / G_{12} = 0,01$.

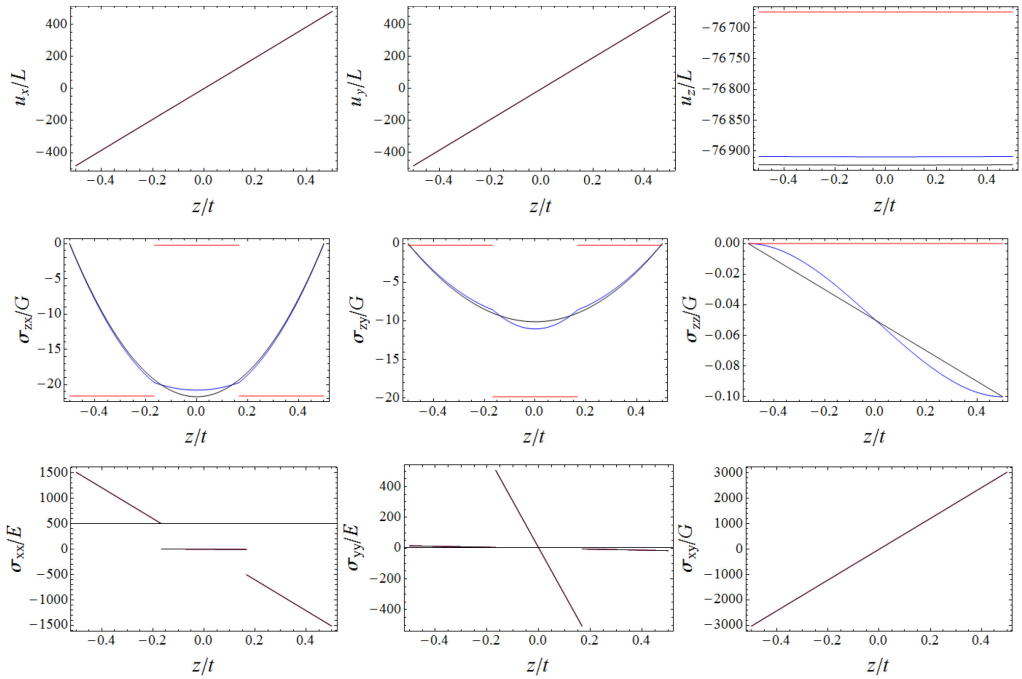

Figure 12. Displacement and stress components for an orthotropic plate with a thickness ratio of 1/250. Red curves are for the standard model, blue for Pagano's model and black for the refined model.

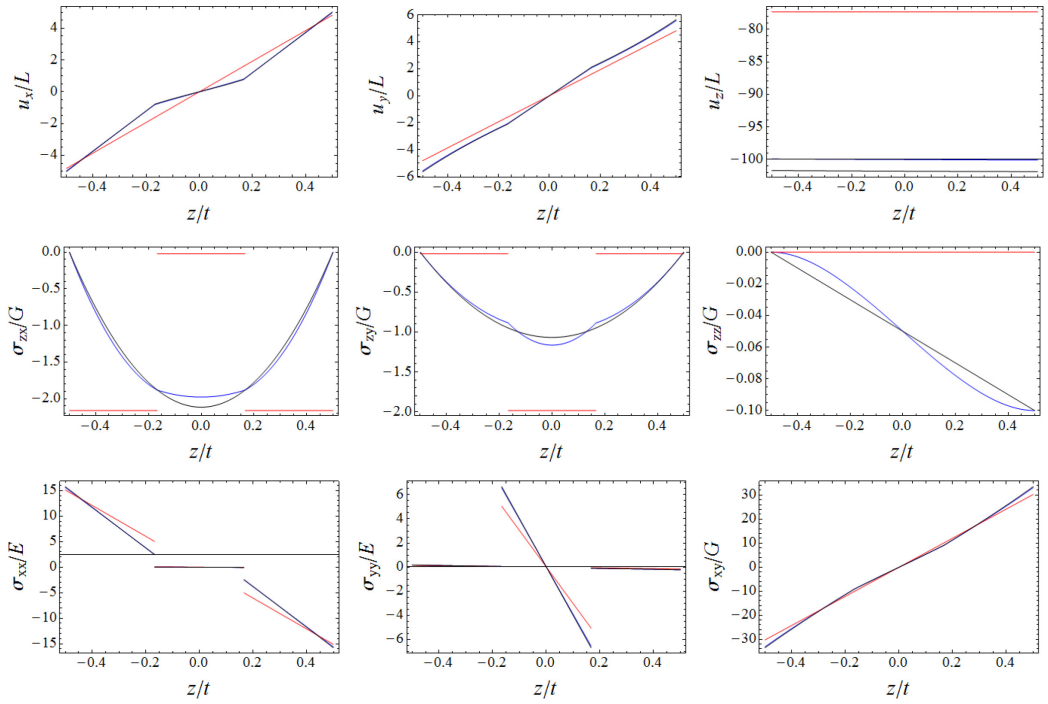

Figure 13. Displacement and stress components for an orthotropic plate with a thickness ratio of 1/25. Red curves are for the standard model, blue for Pagano's model and black for the refined model.

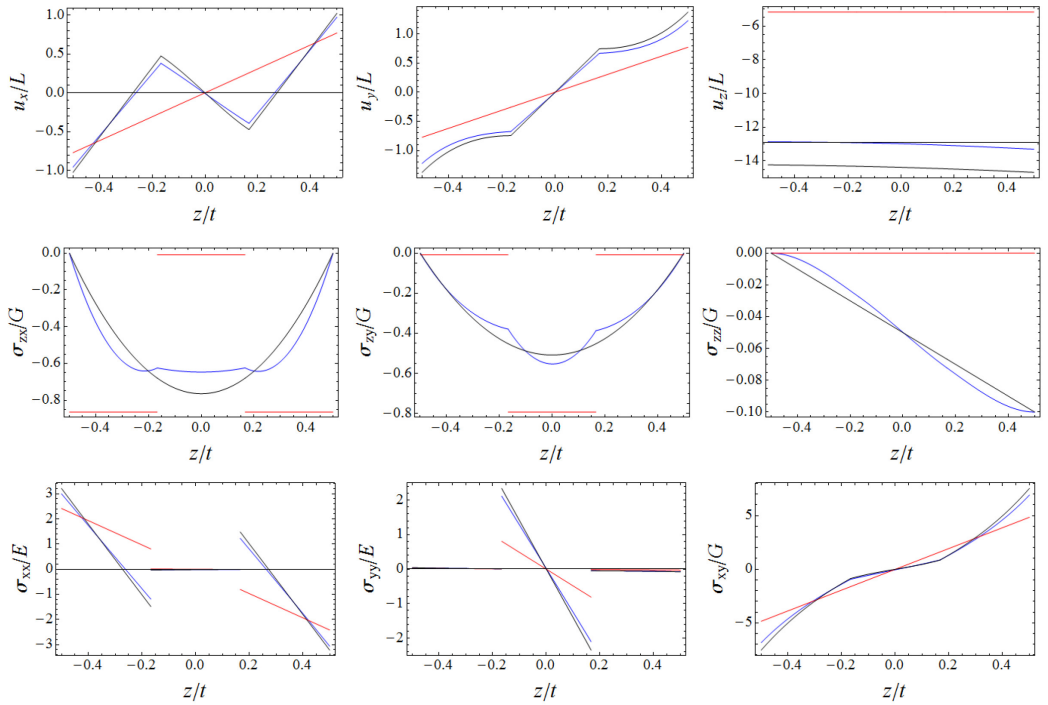

Figure 14. Displacement and stress components for an orthotropic plate with a thickness ratio of 1/10. Red curves are for the standard model, blue for Pagano's model and black for the refined model.

Table 12. Error in the displacement components.

	Refined model			Standard model		
Thickness ratio η	u_x	u_y	u_z	u_x	u_y	u_z
0,004	0,00	0,00	0,00	0,00	0,00	0,00
0,02	0,00	0,00	0,00	0,04	0,04	0,07
0,027	0,00	0,01	0,01	0,08	0,07	0,12
0,04	0,01	0,01	0,02	0,17	0,14	0,23
0,076	0,06	0,06	0,06	0,58	0,33	0,49
0,1	0,12	0,11	0,11	0,83	0,41	0,60
0,2	0,45	0,45	0,36	1,02	0,64	0,80
0,3	0,84	0,92	0,69	1,00	0,86	0,85

Table 13. Error in the continuous stress components.

	Refined model			Standard model		
Thickness ratio η	σ_{zx}	σ_{zy}	σ_{zz}	σ_{zx}	σ_{zy}	σ_{zz}
0,004	0,03	0,06	0,11	0,95	0,95	1
0,02	0,03	0,06	0,11	0,95	0,94	1
0,027	0,04	0,06	0,11	0,95	0,93	1
0,04	0,05	0,06	0,11	0,95	0,90	1
0,076	0,11	0,07	0,10	0,95	0,81	1
0,1	0,16	0,09	0,09	0,94	0,76	1
0,2	0,40	0,22	0,07	0,80	0,63	1
0,3	0,61	0,38	0,10	0,63	0,57	1

Table 14. Error in the discontinuous stress components.

	Refined model			Standard model		
Thickness ratio η	σ_{xx}	σ_{yy}	σ_{xy}	σ_{xx}	σ_{yy}	σ_{xy}
0,004	0,00	0,00	0,00	0,00	0,00	0,00
0,02	0,00	0,01	0,00	0,03	0,07	0,02
0,027	0,00	0,01	0,00	0,06	0,12	0,03
0,04	0,01	0,02	0,01	0,14	0,23	0,06
0,076	0,04	0,07	0,04	0,46	0,50	0,16
0,1	0,09	0,11	0,08	0,68	0,62	0,23
0,2	0,40	0,40	0,39	0,95	0,82	0,41
0,3	0,77	0,86	0,96	0,95	0,88	0,64

The results in Tables 12 to 14 show that the refined model is superior in terms of accuracy to the standard model for nearly all thickness ratios.

The x-, y- and z-directional displacement components of the refined model become less accurate with increasing thickness ratios. However, these components remain more accurate than the standard model for all thickness ratios below 0,3.

As the thickness ratio of the plate becomes smaller, the accuracy of the x- and y-directional shear stress components σ_{zx} and σ_{zy} becomes less accurate. However, they are still more accurate than the standard model at thickness ratios below 0,3. The accuracy of the z-directional stress oscillates around the L_2 norm value of 0,100 as the aspect ratio of the plate is increased.

The normal stresses in the x- and y-axis directions as well as the shear stress in the xy-direction become less accurate with increasing thickness ratios. The refined model is more accurate than the standard model at thickness ratios below 0,2.

It is important to note that the refined model provides significantly improved distributions of the stresses and strains compared to the results of the standard model. This is especially highlighted with the z-directional shear stresses, where the standard model provides a discontinuous form, which would not be physically possible in a continuous laminate. The forms of the refined model's distributions are less accurate with thickness ratios above 0,1. The forms of the distributions are illustrated in Figures 12 - 14.

6.2.4 Cases 4 and 5, results for different material types

Cases 4 and 5 evaluate the effect of the material property ratios by solving the different stress and strain components with different ratios. The materials and values used in this thesis are, in addition to the highly orthotropic material used in the previous evaluations, fir: $\beta = E_2 / E_1 = E_3 / E_1 = 0,059$, $\chi = \nu_{12} / \nu_{32} = \nu_{13} / \nu_{32} = 0,949$ and $\delta = G_{23} / G_{31} = G_{23} / G_{12} = 0,1$, and an isotropic material: $\beta = E_2 / E_1 = E_3 / E_1 = 1$, $\chi = \nu_{12} / \nu_{32} = \nu_{13} / \nu_{32} = 1$ and $\delta = G_{23} / G_{31} = G_{23} / G_{12} = 1$.

The result graphs provided next are solved for cases 4 and 5. In these cases, the length of the plate, L, the modulus of elasticity, E, and the shear modulus, G, are set to be 1. In addition, ply thickness t_i is defined as t / n, loading ratio as $\mu = 1/10$ and Poisson's ratio as $\nu_{32} = 1/3$. The parameters that are given a fixed value in cases 4 and 5 are: number of plies, $n = 3$, aspect ratio, $\gamma = H / L = 1$ and thickness ratio, $\eta = t / L = 1/20$.

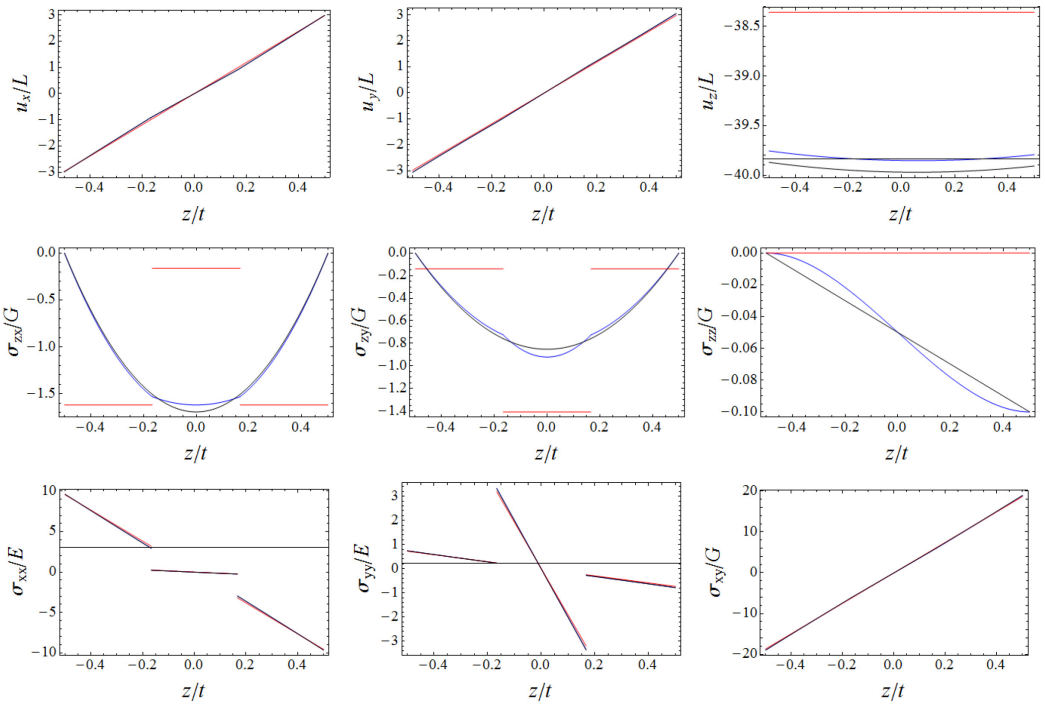

Figure 15. Displacement and stress components for a fir plate with 3 plies. Red curves are for the standard model, blue for Pagano's model and black for the refined model.

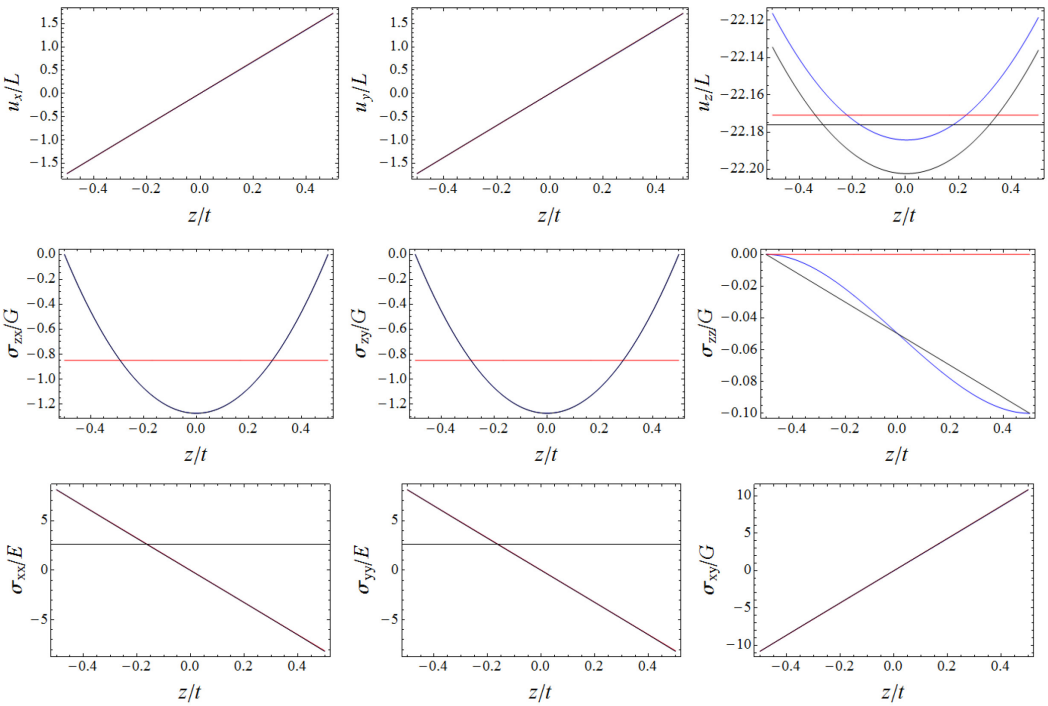

Figure 16. Displacement and stress components for an isotropic plate with 3 plies. Red curves are for the standard model, blue for Pagano's model and black for the refined model.

Table 15. Error in the displacement components.

	Refined model			Standard model		
Material	u_x	u_y	u_z	u_x	u_y	u_z
Orthotropic	0,02	0,02	0,03	0,27	0,20	0,31
Fir	0,00	0,00	0,00	0,03	0,03	0,04
Isotropic	0,00	0,00	0,00	0,01	0,01	0,00

Table 16. Error in the continuous stress components.

	Refined model			Standard model		
Material	σ_{zx}	σ_{zy}	σ_{zz}	σ_{zx}	σ_{zy}	σ_{zz}
Orthotropic	0,06	0,06	0,11	0,95	0,87	1
Fir	0,03	0,05	0,11	0,88	0,69	1
Isotropic	0,00	0,00	0,11	0,41	0,41	1

Table 17. Error in the discontinuous stress components.

	Refined model			Standard model		
Material	σ_{xx}	σ_{yy}	σ_{xy}	σ_{xx}	σ_{yy}	σ_{xy}
Orthotropic	0,01	0,03	0,02	0,21	0,31	0,09
Fir	0,00	0,01	0,00	0,02	0,04	0,01
Isotropic	0,00	0,00	0,00	0,00	0,00	0,01

The results of Tables 15 to 16 show that the accuracy of the models improves when the material becomes less orthotropic and more isotropic. A material with the properties of fir receives significantly more accurate results from all of the models than the highly orthotropic reference material used in the evaluation cases 1 - 3. Still, the use of the highly orthotropic material in these evaluations is justifiable due to its ability to better highlight the effects of the other parameters on the accuracy and form of the distributions.

The accuracy of the refined model is clearly better when compared to the standard model for all of the cases and clear limits are found, below which the refined model is acceptable to use. These findings will be discussed further in the next chapter.

7 Discussion and conclusions

The results from the previous chapter show that the refined model [Freund, 2016] is clearly more accurate than the standard model in practically all of the cases. In fact, the only situation where the refined model was less accurate than the standard model, was for a plate with a thickness ratio of 0,3. However, plates with thicknesses of roughly 1/3 of the length of the plate do not qualify as structures that are thin in one dimension. Another noteworthy aspect of the refined model is that it is, unlike the standard Reissner-Mindlin model, capable of giving a reasonably good estimate of the z-directional stresses. The refined model also provides a notably improved solution for the continuous stress components, which become important when dealing with materials that may break through interlaminate shearing. All in all, judging from the results of these evaluations, the new model has certainly proved its superiority when compared to the standard model. This is especially true with plates that have higher ply numbers and smaller thicknesses, as the error of the model becomes extremely small.

The Reissner-Mindlin model described in Chapter 3 and used as the reference model in the evaluations is relatively inaccurate for materials with greater orthotropy. This is caused by the model's inability to account for the warping of the line segments' normal to the un-deformed plate's mid-plane. However, the model is still significantly better than Kirchhoff plate theory in that the Reissner-Mindlin can account for the relative rotation of the line segments and therefore is better suited for the evaluations in this thesis. The above is confirmed by the evaluations of this thesis and is especially clearly visible in cases 4 and 5.

These findings would indicate that the two-scale plate model would always be preferable to the unmodified Reissner-Mindlin model. The penalty in calculation time when using the refined model was not found to be significant enough to restrict the usage of this model even for heavier calculations. At thickness ratios above 0,1, the use of a more accurate model, such as a three-dimensional elasticity solution should be considered, as the error of the refined model becomes greater than 10% at this point, although the time it takes for a computer to solve the strains and stresses may become quite long with increasing numbers of plies.

Evaluation of the different material types showed that the new model becomes even more accurate when solving cases with materials such as plywood, where the plies show relatively little orthotropy, are identical and only the orientation of the plies varies from layer to layer. As fiber reinforced composite plates are also relatively similar to plywood in terms of structure and properties, this model can be used for cross-stacked symmetric plates with reasonable safety. However, this thesis did not evaluate a case with plies made of two different materials. Plates of this type are found for instance in spacecraft hulls and aircraft wing skin panels. Therefore no evaluation on the suitability of this model for these types of materials can be provided.

During the search for material parameters, there seemed to be only a small amount of good sources available for the material parameters of different types of wood. The sources (Forest Products Laboratory [2001] and Mahoney [2000]) used in the Tables of Chapter 2.2 provided a method to calculate all of the necessary material parameters for certain wood types.

One of the reasons for the small amount of data seems to be the difficulty of defining the exact mechanical properties for wood, as it is a natural material. This means that there is bound to be imperfections in the structure and constitution of the wood caused by different sources such as branches, disease, poor growth years and moisture. All local imperfections have an effect on the total mechanical properties of a material.

The cases presented in this thesis provide a good platform for evaluating the refined model against the standard model and the exact solution. Although the results are relevant and reliable, they are limited to a single and relatively unique plate setup and loading. In real applications, the loads are usually not distributed on the entire plate and they are not perfectly sinusoidal or even uniform. Another limitation of the evaluation is that the loads acting on a plate are not usually centered on the exact geometric center of the plate as is the case presented in this thesis. These shortcomings are acknowledged, but due to the scope of this research, the further evaluation of the model using different cases is left for future research.

It is also to be noted that previous research using the results of Pagano as a benchmark for comparison, has usually been limited to the exact same points as given by Pagano [1969]. This thesis compared the accuracy of the models over the entire thickness of the plate at a greater amount of points in the plate, therefore providing a greater accuracy to the comparison as well as confirming that the refined model's accuracy remains good at any point in the plate.

The major challenge in evaluating further cases is that Pagano's model [Pagano, 1969] is given only for a rectangular plate with simply supported edges and a sinusoidal load distributed on the entire area of the plate. Modifying the exact solution provided by Pagano to allow a localized distributed force such as that caused by a wheel or a box on a plate, would be possible using a sine series with a suitable form. This would be outside the scope of this thesis, as the goal was simply to evaluate the refined model against the standard model and an exact solution, which can be done with sufficient accuracy using the loading case presented in Pagano's article. Still, the use of Pagano's model is acceptable for the evaluations of this thesis, as comparisons with other plate models would not be able to provide equally accurate results for comparison and as only the accuracy of the two-scale model was evaluated.

As this thesis has evaluated the accuracy of the two-scale plate model and found that the model is significantly better than the traditional Reissner-Mindlin model, further research on the new model is warranted. The scope of this thesis is limited to a quite specific case, which leaves many factors that may have an effect on the accuracy of the two-scale model unevaluated. It is therefore recommended that the evaluations be continued with investigations on the effects of edge proximity and different loading cases as well as the effect of aspect ratios that are less than 1. Further research could also be done on the effect of asymmetric lay-ups and plates with plies made of different materials.

Evaluating the effects of different loading cases would involve investigating how a non-sinusoidal, a non-uniform and a localized load affect the accuracy of the two-scale model. In addition, the study on the effects of edge proximity and loading cases could also involve studying the effect of different edge types, such as the fixed and free edges and their effects on the accuracy of the refined model. The research would therefore contain

investigations on how close to the edge can the model still provide accurate results for the stresses and strains, how does the type of edge affect the accuracy and does the type and form of the loads acting on the plate affect the accuracy of the new model.

Similarly, the study on the effects of different materials would be focused on asymmetric lay-ups and plates with plies of different materials and could also include investigation of aspect ratios below 1. The research could also include the effects of plies that are angled at non-perpendicular directions, for instance with a stacking sequence of [0, 45, -45, 45, 0].
The evaluations done in this thesis could also have been improved by expanding the types of materials that were studied to include, for instance, fiber reinforced plastics. These materials are typically extremely anisotropic and would therefore have provided an interesting point of comparison against orthotropic wooden materials.

References

Ashby, M. F.; Jones, D. R. H. 2012. Engineering Materials 1 - An Introduction to Properties, Applications, and Design. Elsevier. ISBN: 978-0-08-096665-6, eISBN: 978-0-0809-6666-3.

Brischetto, S.; Carrera, E.; Demasi, L. 2009. Improved bending analysis of sandwich plates using a zig-zag function. Composite Structures, Volume 89, Issue 3, Pages 408-415, ISSN 0263-8223, DOI:10.1016/j.compstruct.2008.09.001.

Callister, W.; Rethwisch, D. G. 2011. Materials Science and Engineering. John Wiley & Sons. ISBN: 978-0-470-50586-1.

Carrera, E. 2000. A priori vs. a posteriori evaluation of transverse stresses in multilayered orthotropic plates. Composite Structures, Volume 48, Issue 4, Pages 245–260, DOI:10.1016/S0263-8223(99)00112-9.

Carrera, E. 2001. Developments, ideas, and evaluations based upon Reissner's Mixed Variational Theorem in the modeling of multilayered plates and shells. Applied Mechanics Reviews, Volume 54, Issue 4, Pages 301-329, DOI:10.1115/1.1385512.

Carrera, E. 2004. On the use of the Murakami's zig-zag function in the modeling of layered plates and shells. Computers & Structures, Volume 82, Issues 7–8, Pages 541–554, DOI:10.1016/j.compstruc.2004.02.006.

Cho, Y. B.; Averill, R. C. 1997. An improved theory and finite-element model for laminated composite and sandwich beams using first-order zig-zag sublaminate approximations. Composite Structures, Volume 37, Issues 3–4, Pages 281–298, DOI:10.1016/S0263-8223(96)00004-9.

Chou, P. C.; Pagano, N. J. 1967. Elasticity - Tensor, Dyadic, and Engineering Approaches. Dover Publications. ISBN: 978-0-486-66958-8, Electronic ISBN: 978-1-62870-819-6.

Forest Products Laboratory. 2001. Wood Handbook - Wood as an Engineering Material. Revised 1987 version. U.S. Department of Agriculture. Electronic ISBN: 978-1-59124-170-6.

Ferreira, A. J. M.; Roque, C. M. C.; Martins, P. A. L. S. 2003. Analysis of composite plates using higher-order shear deformation theory and a finite point formulation based on the multiquadric radial basis function method. Composites Part B: Engineering, Volume 34, Issue 7, Pages 627-636, ISSN 1359-8368, DOI:10.1016/S1359-8368(03)00083-0.

Freund, J. 2016. Two-scale Reissner Mindlin Plate Model. Manuscript. Aalto University.

Hughes, T. J. R. 1987/2000. Finite Element Method - Linear Static and Dynamic Finite Element Analysis. Dover Publications. ISBN: 978-0-486-41181-1, Electronic ISBN: 978-1-62198-588-4.

Kant, T.; Swaminathan, K. 2002. Analytical solutions for the static analysis of laminated composite and sandwich plates based on a higher order refined theory. Composite Structures, Volume 56, Issue 4, Pages 329-344, ISSN 0263-8223, DOI:/10.1016/S0263-8223(02)00017-X.

Kapuria, S.; Kulkarni, S. D. 2007. An improved discrete Kirchhoff quadrilateral element based on third-order zigzag theory for static analysis of composite and sandwich plates. International Journal for Numerical Methods in Engineering, Volume 69, Issue 9, Pages 1948–1981, ISSN 1097-0207, DOI: 10.1002/nme.1836.

Khandan, R.; Noroozi, S.; Sewell, P.; Vinney, J. 2012. The development of laminated composite plate theories: a review. Journal of Material Sciences, Volume 47, Issue 16, Pages 5901-5910, DOI 10.1007/s10853-012-6329-y.

Lee, D. G.; Suh, N. P. 2006. Axiomatic Design and Fabrication of Composite Structures - Applications in Robots, Machine Tools, and Automobiles. Oxford University Press. ISBN: 978-0-19-517877-7, Electronic ISBN: 978-1-61344-947-9.

Mahoney, W. D. 2000. Wood Engineering Handbook. 2nd edition. BNI Building News. ISBN: 978-1-55701-375-0, Electronic ISBN: 978-1-62870-269-9.

Mantari, J. L.; Oktem, A. S.; Guedes Soares, C. 2012. A new higher order shear deformation theory for sandwich and composite laminated plates. Composites Part B: Engineering, Volume 43, Issue 3, Pages 1489-1499, ISSN 1359-8368, DOI: /10.1016/j.compositesb.2011.07.017.

Matsunaga, H. 2002. Assessment of a global higher-order deformation theory for laminated composite and sandwich plates. Composite Structures, Volume 56, Issue 3, Pages 279-291, ISSN 0263-8223, DOI:10.1016/S0263-8223(02)00013-2.

Niu, M. C. Y. 1992. Composite Airframe Structures - Practical Design Information and Data. 3rd edition. AD Adaso/Adastra Engineering LLC. ISBN: 978-962-7128-11-3, Electronic ISBN: 978-1-61344-656-0.

Pagano, N.J. 1969. Exact solutions for rectangular bidirectional composites and sandwich plates. Journal of composite materials, Volume 4, Issue 1, pages 20-34.

Reddy, J. N. 1997/2004. Mechanics of laminated composite plates and shells: theory and analysis. CRC Press. ISBN: 0-8493-1592-1.

Smith, R. C. 2005. Smart Material Systems - Model Development. Society for Industrial and Applied Mathematics. ISBN: 978-0-89871-583-5, Electronic ISBN: 978-1-62870-858-5.

List of appendices

Appendix A.1. Derivation of the stress-strain relation with the $\sigma_{zz} = 0$ assumption

The derivation of the modified stress-strain relation begins from equation (A.1), which is shown below.

$$\begin{Bmatrix} \sigma_{11} \\ \sigma_{22} \\ \sigma_{33} \end{Bmatrix} = \begin{bmatrix} \frac{1}{E_1} & \frac{-\nu_{21}}{E_2} & \frac{-\nu_{31}}{E_3} \\ \frac{-\nu_{12}}{E_1} & \frac{1}{E_2} & \frac{-\nu_{32}}{E_3} \\ \frac{-\nu_{13}}{E_1} & \frac{-\nu_{23}}{E_2} & \frac{1}{E_3} \end{bmatrix}^{-1} \begin{Bmatrix} \varepsilon_{11} \\ \varepsilon_{22} \\ \varepsilon_{33} \end{Bmatrix} = \mathbf{E} \begin{Bmatrix} \varepsilon_{11} \\ \varepsilon_{22} \\ \varepsilon_{33} \end{Bmatrix} \tag{A.1}$$

Assuming that there are no stresses in the direction of the ply's z-axis does not affect the shear stresses or strains, which means that the shear modulus matrix $\mathbf{G}$ is not affected by this assumption and does therefore not require any modifications.

Equation (A.1) can be multiplied with the inverse of $\mathbf{E}$ to provide the following equation

$$\begin{Bmatrix} \varepsilon_{11} \\ \varepsilon_{22} \\ \varepsilon_{33} \end{Bmatrix} = \begin{Bmatrix} \frac{\sigma_{11}}{E_1} - \frac{\nu_{21}\sigma_{22}}{E_2} - \frac{\nu_{31}\sigma_{33}}{E_3} \\ \frac{-\nu_{12}\sigma_{11}}{E_1} + \frac{\sigma_{22}}{E_2} - \frac{\nu_{32}\sigma_{33}}{E_3} \\ \frac{-\nu_{13}\sigma_{11}}{E_1} - \frac{\nu_{23}\sigma_{22}}{E_2} + \frac{\sigma_{33}}{E_3} \end{Bmatrix}. \tag{A.2}$$

The assumption that $\sigma_{zz} = 0$ is now inserted to equation (A.2)

$$\begin{Bmatrix} \varepsilon_{11} \\ \varepsilon_{22} \\ \varepsilon_{33} \end{Bmatrix} = \begin{Bmatrix} \frac{\sigma_{11}}{E_1} - \frac{\nu_{21}\sigma_{22}}{E_2} \\ \frac{-\nu_{12}\sigma_{11}}{E_1} + \frac{\sigma_{22}}{E_2} \\ \frac{-\nu_{13}\sigma_{11}}{E_1} - \frac{\nu_{23}\sigma_{22}}{E_2} \end{Bmatrix}. \tag{A.3}$$

The resulting equation can be divided into the following equations

$$\begin{Bmatrix} \varepsilon_{11} \\ \varepsilon_{22} \end{Bmatrix} = \begin{bmatrix} \frac{1}{E_1} & -\frac{\nu_{21}}{E_2} \\ -\frac{\nu_{12}}{E_1} & \frac{1}{E_2} \end{bmatrix} \begin{Bmatrix} \sigma_{11} \\ \sigma_{22} \end{Bmatrix} \tag{A.4}$$

and

$$\varepsilon_{33} = -\frac{\nu_{13}\sigma_{11}}{E_1} - \frac{\nu_{23}\sigma_{22}}{E_2}, \tag{A.5}$$

of which the latter is not needed in calculations.

Equation (A.4) can now be modified to provide the equations for stresses

$$\begin{Bmatrix} \sigma_{11} \\ \sigma_{22} \\ \sigma_{33} \end{Bmatrix} = \frac{1}{1-\nu_{21}\nu_{12}} \begin{bmatrix} E_1 & \nu_{21}E_1 & 0 \\ \nu_{12}E_2 & E_2 & 0 \\ 0 & 0 & 0 \end{bmatrix} \begin{Bmatrix} \varepsilon_{11} \\ \varepsilon_{22} \\ \varepsilon_{33} \end{Bmatrix} = \mathbf{E} \begin{Bmatrix} \varepsilon_{11} \\ \varepsilon_{22} \\ \varepsilon_{33} \end{Bmatrix}. \tag{A.6}$$

The resulting equation is of such form that the stresses acting in the 33-direction are 0, no matter what the strains in the plate are. To further simplify the notation for further calculation, the Young's modulus terms in matrix **E** are shortened in the manner shown in equations (A.7) to provide a more compact form.

$$E_{11} = \frac{E_1}{1-\nu_{21}\nu_{12}},$$

$$E_{12} = \frac{\nu_{21}E_1}{1-\nu_{21}\nu_{12}},$$

$$E_{21} = \frac{\nu_{12}E_2}{1-\nu_{21}\nu_{12}}, \tag{A.7}$$

$$E_{22} = \frac{E_2}{1-\nu_{21}\nu_{12}}$$

and

$$\mathbf{E} = \begin{bmatrix} E_{11} & E_{12} & 0 \\ E_{21} & E_{22} & 0 \\ 0 & 0 & 0 \end{bmatrix}.$$

Appendix A.2. The derivation of the constitutive equation

The equation of the elasticity dyad is

$$\ddot{\vec{E}} = \begin{Bmatrix} \vec{e}_1\vec{e}_1 \\ \vec{e}_2\vec{e}_2 \\ \vec{e}_3\vec{e}_3 \end{Bmatrix}^T \mathbf{E} \begin{Bmatrix} \vec{e}_1\vec{e}_1 \\ \vec{e}_2\vec{e}_2 \\ \vec{e}_3\vec{e}_3 \end{Bmatrix} + \begin{Bmatrix} \vec{e}_1\vec{e}_2 + \vec{e}_2\vec{e}_1 \\ \vec{e}_2\vec{e}_3 + \vec{e}_3\vec{e}_2 \\ \vec{e}_3\vec{e}_1 + \vec{e}_1\vec{e}_3 \end{Bmatrix}^T \mathbf{G} \begin{Bmatrix} \vec{e}_1\vec{e}_2 + \vec{e}_2\vec{e}_1 \\ \vec{e}_2\vec{e}_3 + \vec{e}_3\vec{e}_2 \\ \vec{e}_3\vec{e}_1 + \vec{e}_1\vec{e}_3 \end{Bmatrix}, \tag{A.8}$$

where

$$\mathbf{E} = \begin{bmatrix} \dfrac{E_1}{1-\nu_{21}\nu_{12}} & \dfrac{\nu_{21}E_1}{1-\nu_{21}\nu_{12}} & 0 \\ \dfrac{\nu_{12}E_2}{1-\nu_{21}\nu_{12}} & \dfrac{E_2}{1-\nu_{21}\nu_{12}} & 0 \\ 0 & 0 & 0 \end{bmatrix} \tag{A.9}$$

and

$$\mathbf{G} = \begin{bmatrix} G_{12} & 0 & 0 \\ 0 & G_{23} & 0 \\ 0 & 0 & G_{31} \end{bmatrix}. \tag{A.10}$$

The ply coordinate system unit vectors $\vec{e}_1$, $\vec{e}_2$ and $\vec{e}_3$ in equation (A.8) need to be converted to the plate coordinate system. This can be achieved with the use of the following conversion matrix

$$\begin{Bmatrix} \vec{e}_1 \\ \vec{e}_2 \\ \vec{e}_3 \end{Bmatrix} = \begin{bmatrix} \mathrm{c} & \mathrm{s} & 0 \\ -\mathrm{s} & \mathrm{c} & 0 \\ 0 & 0 & 1 \end{bmatrix} \begin{Bmatrix} \vec{e}_x \\ \vec{e}_y \\ \vec{e}_z \end{Bmatrix}. \tag{A.11}$$

In which, $\mathrm{c} = \cos(\alpha)$ and $\mathrm{s} = \sin(\alpha)$.

To further simplify the notation in following equations, the Young's modulus terms in matrix **E** are shortened in the manner shown in equations (A.7) to provide a more compact form.

Using the simplifications and definitions given in equations (A.8) to (A.11), and equation (A.7), the plate coordinate system elasticity dyad for the standard model can be derived. This is done through substitution of equation (A.11) into equation (A.8) and calculating the new matrices to end up with the form shown in equation (A.12).

$$\ddot{\vec{E}} = \begin{Bmatrix} \vec{e}_x\vec{e}_x \\ \vec{e}_y\vec{e}_y \\ \vec{e}_x\vec{e}_y + \vec{e}_y\vec{e}_x \\ \vec{e}_y\vec{e}_z + \vec{e}_z\vec{e}_y \\ \vec{e}_z\vec{e}_x + \vec{e}_x\vec{e}_z \end{Bmatrix}^T \begin{bmatrix} S_1 & S_3 & S_7 & 0 & 0 \\ S_3 & S_2 & S_8 & 0 & 0 \\ S_7 & S_8 & S_4 & 0 & 0 \\ 0 & 0 & 0 & S_5 & S_9 \\ 0 & 0 & 0 & S_9 & S_6 \end{bmatrix} \begin{Bmatrix} \vec{e}_x\vec{e}_x \\ \vec{e}_y\vec{e}_y \\ \vec{e}_x\vec{e}_y + \vec{e}_y\vec{e}_x \\ \vec{e}_y\vec{e}_z + \vec{e}_z\vec{e}_y \\ \vec{e}_z\vec{e}_x + \vec{e}_x\vec{e}_z \end{Bmatrix} \tag{A.12}$$

The 3D elasticity dyad is of similar form and is written as follows

$$\ddot{\vec{E}} = \begin{Bmatrix} \vec{e}_x\vec{e}_x \\ \vec{e}_y\vec{e}_y \\ \vec{e}_z\vec{e}_z \\ \vec{e}_x\vec{e}_y + \vec{e}_y\vec{e}_x \\ \vec{e}_y\vec{e}_z + \vec{e}_z\vec{e}_y \\ \vec{e}_z\vec{e}_x + \vec{e}_x\vec{e}_z \end{Bmatrix}^T \begin{bmatrix} S_1 & S_3 & S_{11} & S_7 & 0 & 0 \\ S_3 & S_2 & S_{12} & S_8 & 0 & 0 \\ S_{11} & S_{12} & S_{10} & S_{13} & 0 & 0 \\ S_7 & S_8 & S_{13} & S_4 & 0 & 0 \\ 0 & 0 & 0 & 0 & S_5 & S_9 \\ 0 & 0 & 0 & 0 & S_9 & S_6 \end{bmatrix} \begin{Bmatrix} \vec{e}_x\vec{e}_x \\ \vec{e}_y\vec{e}_y \\ \vec{e}_z\vec{e}_z \\ \vec{e}_x\vec{e}_y + \vec{e}_y\vec{e}_x \\ \vec{e}_y\vec{e}_z + \vec{e}_z\vec{e}_y \\ \vec{e}_z\vec{e}_x + \vec{e}_x\vec{e}_z \end{Bmatrix}. \tag{A.13}$$

The terms in equations (A.12) and (A.13) are

$$S_1 = E_{11}c^4 + 2E_{12}s^2c^2 + E_{22}s^4 + 4G_{12}c^2s^2 \ ,$$

$$S_3 = E_{11}c^2s^2 + \left(c^4 + s^4\right)E_{12} + E_{22}c^2s^2 - 4G_{12}c^2s^2 \,,$$

$$S_7 = E_{11}c^3s + E_{12}\left(-c^3s + cs^3\right) - E_{22}cs^3 - 2G_{12}c^3s + 2G_{12}cs^3 \,,$$

$$S_2 = E_{11}s^4 + 2E_{12}s^2c^2 + E_{22}c^4 + 4G_{12}c^2s^2 \,,$$

$$S_8 = E_{11}cs^3 + E_{12}\left(-cs^3 + c^3s\right) - E_{22}c^3s + 2G_{12}c^3s - 2G_{12}cs^3 \,, \qquad \text{(A.14)}$$

$$S_4 = E_{11}c^2s^2 - 2E_{12}s^2c^2 + E_{22}c^2s^2 - 2G_{12}c^2s^2 + G_{12}s^4 + G_{12}c^4 \,,$$

$$S_5 = G_{23}c^2 + G_{31}s^2 \,,$$

$$S_6 = G_{23}s^2 + G_{31}c^2$$

and

$$S_9 = G_{31}sc - G_{23}cs \,.$$

The terms presented above correspond to those that are shown by Reddy [2004, pages 96-97].

The additional terms from the three-dimensional matrix (A.13) are as follows

$$S_{10} = E_{33}$$

$$S_{11} = E_{23}s^2 + E_{13}c^2 \,, \qquad \text{(A.15)}$$

$$S_{12} = E_{23}c^2 + E_{13}s^2 \ ,$$

and

$$S_{13} = E_{13}cs - E_{23}cs$$